metals

Review

# Microstructures and Mechanical Properties of Steels and Alloys Subjected to Large-Strain Cold-to-Warm Deformation

**Anastasiia Dolzhenko [1], Marina Tikhonova [1], Rustam Kaibyshev [2] and Andrey Belyakov [1,*]**

[1] Laboratory of Mechanical Properties of Nanostructured Materials and Superalloys, Belgorod State University, 308015 Belgorod, Russia; dolzhenko_a@bsu.edu.ru (A.D.); tikhonova@bsu.edu.ru (M.T.)
[2] Russian State Agrarian University—Moscow Timiryazev Agricultural Academy (RSAU-MTAA), 127550 Moscow, Russia; kajbyshev@rgau-msha.ru
* Correspondence: belyakov@bsu.edu.ru

**Abstract:** The effect of large-strain cold-to-warm deformation on the microstructures and mechanical properties of various steels and alloys is critically reviewed. The review is mainly focused on the microstructure evolution, whereas the deformation textures are cursorily considered without detailed examination. The deformation microstructures are considered in a wide strain range, from early straining to severe deformations. Such an approach offers a clearer view of how the deformation mechanisms affect the structural changes leading to the final microstructures evolved in large strains. The general regularities of microstructure evolution are shown for different deformation methods, including conventional rolling/swaging and special techniques, such as equal channel angular pressing or torsion under high pressure. The microstructural changes during deformations under different processing conditions are considered as functions of total strain. Then, some important mutual relationships between the microstructural parameters, e.g., grain size vs. dislocation density, are revealed and discussed. Particular attention is paid to the mechanisms of microstructure evolution that are responsible for the grain refinement. The development of an ultrafine-grained microstructure during large strain deformation is considered in terms of continuous dynamic recrystallization. The regularities of the latter are discussed in comparison with conventional (discontinuous) dynamic recrystallization and grain subdivision (fragmentation) phenomenon. The structure–property relations are quantitatively represented for the structural strengthening, taking into account various mechanisms of dislocation retardation.

**Keywords:** steels and alloys; large plastic strain; deformation microstructure; dislocation substructure; work hardening; strengthening mechanism



**Citation:** Dolzhenko, A.; Tikhonova, M.; Kaibyshev, R.; Belyakov, A. Microstructures and Mechanical Properties of Steels and Alloys Subjected to Large-Strain Cold-to-Warm Deformation. *Metals* **2022**, *12*, 454. https://doi.org/10.3390/met12030454

Academic Editors: Hongliang Yi and Pasquale Cavaliere

Received: 9 February 2022
Accepted: 3 March 2022
Published: 8 March 2022



## 1. Introduction

The deformation microstructures that evolve in steels and alloys by large-strain cold-to-warm working are of great importance for materials scientists and mechanical engineers. Almost all established thermomechanical treatments and novel metal-forming processing methods involve plastic deformation to rather large strains under various conditions [1–3]. Needless to say, the mechanical properties of the final products are highly dependent on the microstructural state, which, in turn, is controlled by preceding plastic working. Strength and plasticity are perhaps the most sensitive to the deformation microstructures among many other microstructure-dependent mechanical properties [1,4].

Commonly, cold-to-warm working strengthens metallic materials, whereas plasticity degrades [5]. The main mechanisms of structural strengthening, which are controlled by plastic deformation, include grain refinement (grain-size strengthening) and increasing the dislocation density (dislocation strengthening or work hardening) [6–8]. The regularities of microstructure evolution, including the change in the grain size and the dislocation density during plastic deformation at elevated temperatures, i.e., under hot working conditions, have been fairly clarified in a number of papers [9–13]. On the other hand, the deformation microstructures evolved under conditions of cold-to-warm working have not been quantitatively generalized. This gap in the knowledge is associated with practical difficulty in attaining sufficiently large strains to achieve the steady-state deformation behavior when the deformation microstructures are solely controlled by processing conditions. In past decades, several special techniques have been developed to realize severe plastic deformation at low-to-moderate temperatures [14–20]. Among those techniques, torsion under high pressure and equal channel angular pressing (ECAP) are the most famous ones [21–23]. The grain size in structural materials can be reduced down to tens of nanometers by severe deformation. Several reviews dealt with the nanostructured materials obtained by severe plastic deformation, including special reviews on high-pressure torsion (HPT) [7,15,23]. It is commonly agreed that severe deformation is accompanied by a kind of continuous dynamic recrystallization. The latter involves the progressive transformation of the strain-induced subgrains into ultrafine grains as a result of gradual increase in the angular misorientations between the deformation subgrains [14,24–27]. However, the sequence of structural changes, namely the mechanisms of submicrocrystalline or nanocrystalline microstructure evolution during large strain deformation are still a subject of some debates. The most of specific severe plastic deformation techniques are rather cumbersome procedures that are used for research purpose only; however, some of them, such as ECAP-Conform [28], accumulative roll-bonding [29], and multiple forging [30], can be utilized for sizeable semi-products.

The aim of the present review is to synthesize briefly the progress in recent studies on the deformation microstructures and their effect on mechanical properties of various metallic materials subjected to large strain deformation at relatively low temperatures. Following the outline of frequently used techniques of large strain deformation and modern methods for structural investigation in Section 2, the regularities of microstructure and texture evolution are treated in Sections 3 and 4, respectively. Special attention is paid to the relationships between the main microstructural parameters and true strain. Then, the mechanical properties of largely strained steels and alloys are discussed in Section 5, focusing on the mechanisms of microstructural strengthening and their combinations and interactions. Finally, the effect of processing conditions is summarized in Section 6, followed by the authors' viewpoint on the further progress in the field.

## 2. Large Strain Deformation

### *2.1. Processing Methods*

An interest in producing ultrafine-grained metallic materials with beneficial combination of mechanical properties encouraged the development of a number of special techniques of severe plastic deformation. It is believed that substantial grain refinement can be achieved after large strains at relatively low deformation temperatures [14]. Following the principles outlined by Segal et al. [16], the ECAP method has been developed and used successfully for over three decades (Figure 1a). It has been frequently used for processing soft materials and has become quite popular [15,22]. The sample is pressed through two intersecting channels of the same shape and cross-section, and the equivalent strain is evaluated as follows [15]:

$$\varepsilon = \{2\cot[0.5(\phi + \psi)] + \psi\,\mathrm{cosec}[0.5(\phi + \psi)]\}/\sqrt{3} \tag{1}$$

where $\phi$ and $\psi$ are the angle between channels and the curvature of channel intersection. Sequential pressing of a sample through the die results in a large total strain, while the shape of the sample does not change.

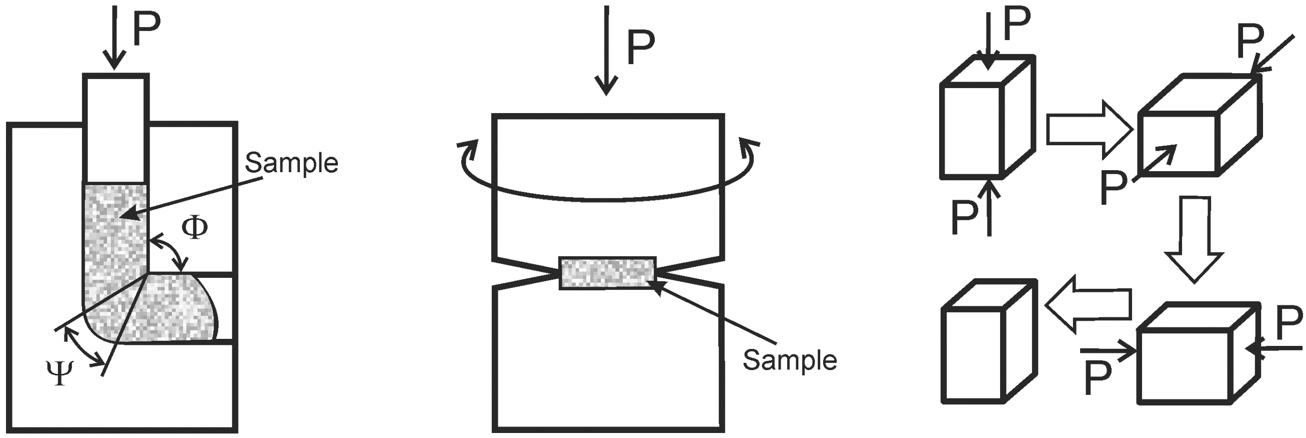


(**a**) (**b**) (**c**)

**Figure 1.** Large strain deformation by equal channel angular pressing, ECAP (**a**); high-pressure torsion, HPT (**b**); and multiple forging (**c**).

Another frequently used technique is torsion under high axial pressure (high pressure torsion, HPT), which was originally proposed by Bridgman (Figure 1b) [23]. The strain imposed on a disc-shaped specimen depends on its thickness ($t$), radius ®, and rotation angle ($\theta$) [31]:

$$\varepsilon = (\theta R)/(t\sqrt{3}) \tag{2}$$

An additional compressive strain must be added to the total strain if the specimen thickness is reduced during HPT. Compared to ECAP, the HPT does not require costly equipment and can be applied for a wide variety of metals and alloys, including hard-to-deform materials; however, it can hardly be used for sizeable samples. Besides ECAP and HPT, a number of other specific techniques, e.g., cyclic extrusion compression, accumulative roll-bonding, friction stir processing, continuous cyclic bending, repetitive corrugation and straightening, mechanical milling, etc., have been methods of severe plastic deformation [18,19,32–37].

It should be noted that conventional metal-forming techniques also allow us to attain large strain deformation. Multi-axial multiple forging seems to be the simplest and easiest realized method for large strain processing (Figure 1c). Damascus swords and armor processed by redundant forging are among amazing examples of largely strained products [38]. Scientific interest in multiple forging was resumed in the early 1990s that was motivated by outstanding properties of ultrafine grained metals and alloys produced by severe plastic deformation [39]. The principal advantage of this method is a feasibility of obtaining the true stress–true strain diagram, which is sometimes indispensable for adequate interpretation of obtained results [25,40]. Furthermore, the total strain is easily estimated by a summation of the strain in each forging pass that is determined by the ratio of the initial to the final dimension of the specimen, i.e., $\varepsilon = \ln (H_i/H_f)$. Uniaxial processing methods, such as rolling, drawing, and swaging, can be also used for large-strain processing [41]. These methods are based on standard tools and are easy to use in applications.

### *2.2. Microstructure Characterization*

Besides conventional light microscopy, several diffraction research methods are widely used to characterize the deformation microstructures in cold/warm-worked metallic materials. Among those, transmission electron microscopy (TEM), scanning electron microscopy (SEM), and X-ray diffraction analysis (XRD) should be mentioned as the most frequently applied. TEM and SEM equipped with an electron back-scattering diffraction pattern (EBSP) analyzer incorporating an orientation imaging microscopy (OIM) system offer a number of advantages over the others. These techniques make it possible to observe the fine structural elements with high resolution. Obtaining Kikuchi-diffraction with converged beam technique in TEM [42] allows for the precise investigation of crystallographic orientations of nanostructural objects evolved by large strain deformation [43]. The development of automatic analyzing system for EBSP opens up quite new possibilities for investigation of deformation microstructures [44].

Currently, EBSP is considered as a fundamentally new type of microscopy [45]. Its essence lies in the systematic measurement of the crystallographic orientations at various points of the selected surface area of the sample. The resulting maps make it possible to reveal the boundaries of grains/subgrains and to determine the grain/subgrain boundary misorientations. This, in turn, contributes to a more adequate interpretation of the microstructure, as compared to light microscopy and ordinary SEM, where the nature of boundaries often has to be judged only by indirect signs. In addition, EBSP allows us to obtain the spectrum of misorientations, which is one of the most important characteristics of deformation microstructures. The successful development of EBSP apparatus over the past decades has made it possible to apply it to the study of very complex objects, such as nanostructured steels and alloys. Presently, the EBSP method is one of the most frequently used methods to study almost all microstructural aspects of thermomechanical treatment, including phase transformations [46]. Recent achievements in the field suggest that the EBSP technique can be used to characterize the dislocation substructure [47]. Combined with a focused ion beam, EBSP provides insight into spatial dislocation distribution [48]. There is no doubt that EBSP is the most powerful and promising technique presently available for microstructure characterization.

The methods of X-ray diffraction are commonly used for texture investigation in various metallic materials, including those subjected to large strain deformation. X-ray diffraction gives adequate information about the general texture on the macroscale, as is considered later in Section 4. Note here that modern X-ray techniques possess enhanced resolution. A recently developed method for calculating the orientation distribution function makes it possible to carry out a quantitative analysis of the microtexture of individual grains [49]. Besides electron microscopy and X-ray diffractometry, a new method of atom-probe tomography has been recently utilized to analyze solute clustering and segregation occurring during deformation [50]. These data provide new insights about the mechanisms controlling dynamic precipitation and segregation at deformation grain boundaries.

## 3. Microstructure Evolution

The deformation microstructures evolved during large-strain cold-to-warm working depending on the processing route [51,52]. The change in the strain path may have a significant effect on the kinetics of microstructure evolution and the morphology of the developed microstructure and is considered in Section 3.3. Here, the general regularities of microstructure evolution are qualitatively introduced neglecting the effect of deformation method. The deformation microstructures evolved in steel samples subjected to bar rolling/swaging at ambient temperature are shown in Figure 2 as typical examples to illustrate the microstructural changes. The sequence of microstructural changes during large strain deformation at relatively low temperatures can be summarized as follows [53].

Commonly, an increase in the dislocation density with straining is accompanied by dynamic recovery. Recovery assists the dislocation rearrangement, leading to the development of cell blocks separated by dense dislocation walls. Then the deformation microbands appear at rather large strains (Figure 2a). Further straining results in the development of a layered microstructure composed of highly elongated grains/subgrains along the direction of metal flow that is more pronounced in ductile materials susceptible to dynamic recovery (Figure 2b). The deformation microstructure after severe plastic straining consists of elongated ultrafine grains (Figure 2c). The latter ones readily evolve along the microshear bands and at their intersections [54]. Increasing the number density of microshear bands may be a factor of a progressive increase in the volume fraction of the ultrafine grains during cold-to-warm working.

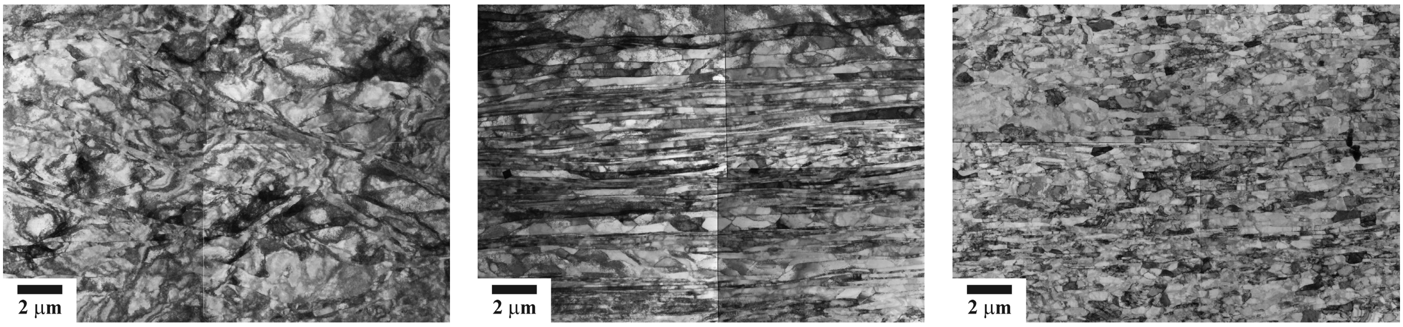


(**a**) (**b**) (**c**)

**Figure 2.** Deformation microstructures evolved in Fe-22%Cr-3%Ni steel subjected to cold bar rolling to a strain of 1.0 (**a**); cold bar rolling to a strain of 2, followed by swaging to total strain of 3.2 (**b**); or cold bar rolling to a strain of 2.0, followed by swaging top total strain of 4.4 (**c**) [53].

A decrease in stacking fault energy (SFE) promotes the development of microshear bands and, therefore, advances the evolution of ultrafine grained microstructure [55]. Frequent development of microshear bands (MSBs) consisting of elongated ultrafine grains/subgrains was observed in an austenitic stainless steel subjected to warm rolling to moderate strains of 2 to 3 (Figure 3). Note that the deformation grains/subgrains became finer while their boundary/sub-boundary misorientations increased with an increase in strain. The same accelerating effect on the microstructure evolution during cold-to-warm working can be achieved by the solid solution and/or dispersion strengthening [56]. A Cu-Ni-P alloy after solution treatment or solution treatment, followed by low temperature aging, was characterized by a much finer cold-rolled microstructure compared to pure copper and the same alloy subjected to solution treatment followed by high temperature aging (Figure 4). The grain refinement in these samples was assisted by the development of deformation twinning, and microshear banding resulted from rapid strain hardening at early deformation.

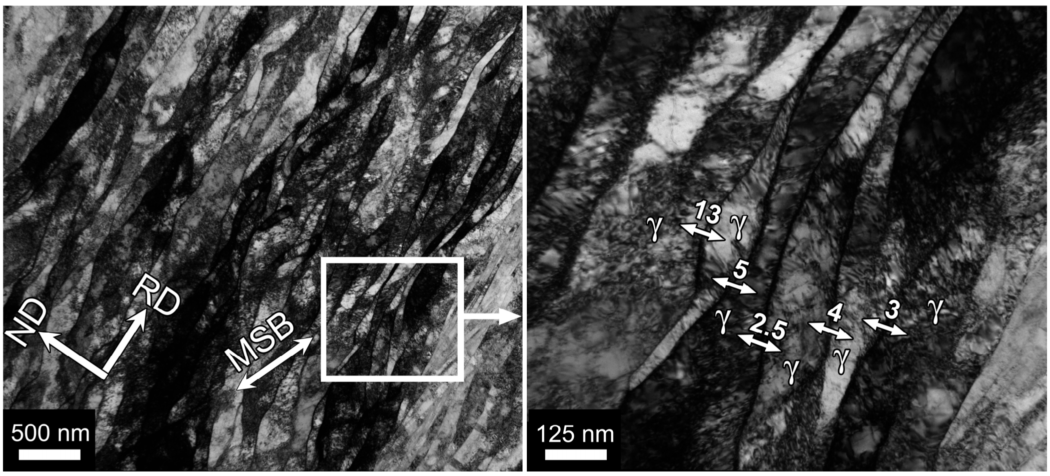


(**a**)

**Figure 3.** *Cont.*

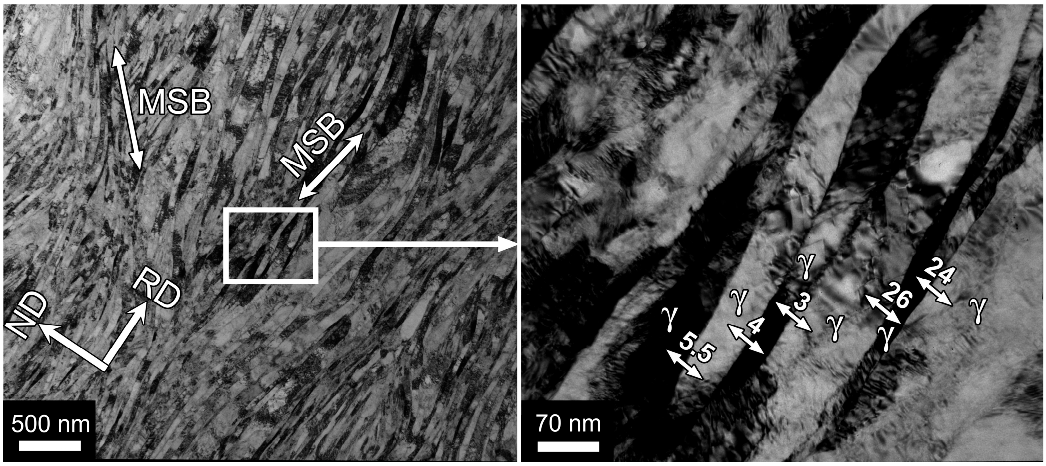


(**b**)

**Figure 3.** Deformation microstructures in a 316L-type steel subjected to rolling at 573 K to a strain of 2 (**a**) and 3 (**b**) [55].

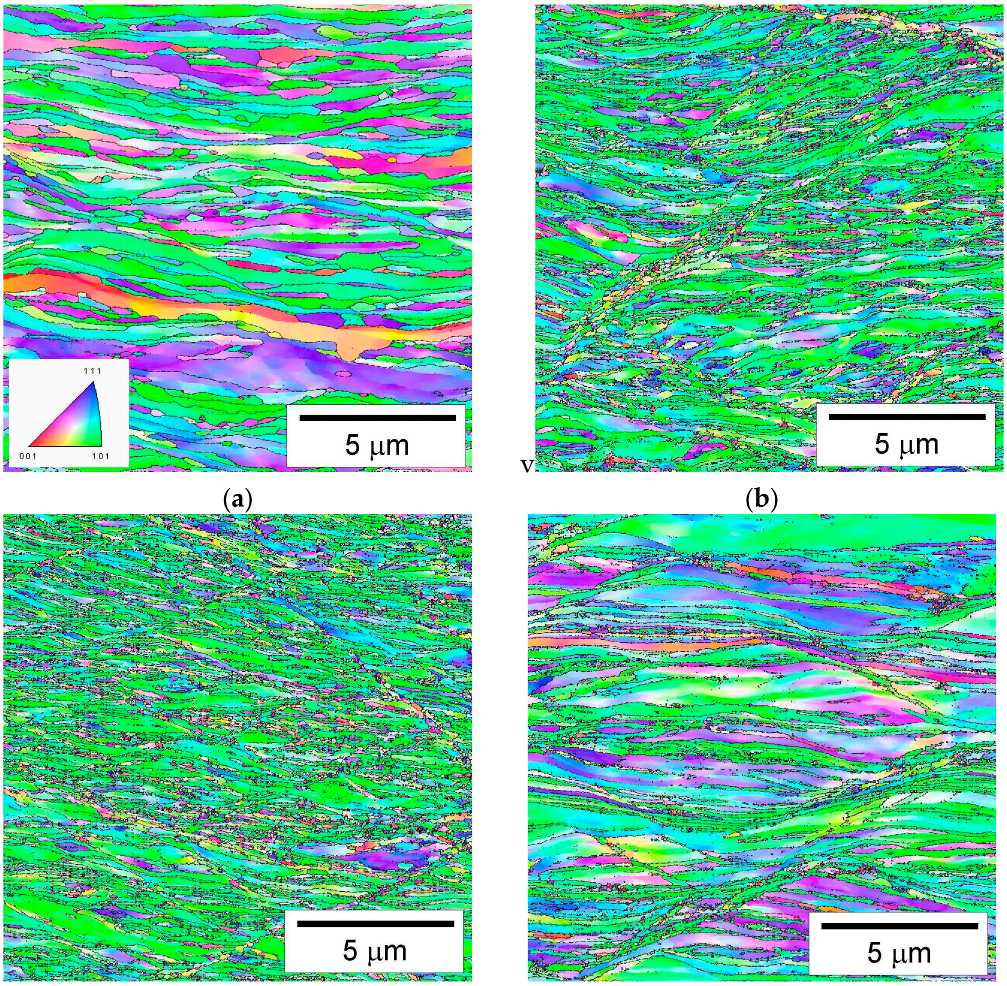


**Figure 4.** Deformation microstructures evolved by cold rolling to a strain of 5 in a pure copper (**a**) and a Cu-1.5%Ni-0.3%P alloy after solution treatment (**b**), or solution treatment and aging at 673 K (**c**), or solution treatment and aging at 873 K (**d**) [56]. Inverse pole figures relate to the normal direction (vertical).

The new ultrafine grains developed in severely strained metals and alloys result from gradual increase in the misorientations between subgrains evolved at preceding strains that is a kind of continuous reactions commonly referred to as continuous dynamic recrystallization [57]. Similar to continuous static recrystallization [58], early observations of continuous dynamic recrystallization were carried out at hot deformation of aluminum alloys with dispersed particles [59]. The dispersed particles restricted the grain growth, leading to the fine-grained microstructure, owing to a progressive increase in misorientations between the deformation subgrains. Then continuous dynamic recrystallization was frequently observed during hot working in single-phase metallic materials susceptible to dynamic recovery, such as ferritic steels [60,61]. Decreasing the deformation temperature from hot to warm/cold working was accompanied by increasing the role of deformation microbands in the new grain development [61] similar to that in fcc-metals/alloys discussed above. The deformation microstructures in hcp-metals/alloys are closely connected with the operating deformation mechanisms [62,63]. The development of continuous dynamic recrystallization in Mg and its alloys during warm working was attributed to cross slip, whereas that during cold working was promoted by deformation twinning.

Rybin [64] suggested a linear function between the strain and the maximal misorientation ($\theta_{max}$) of the strain-induced boundaries as follows:

$$\theta_{max} = A\,(\varepsilon - \varepsilon_0) \tag{3}$$

where A is a temperature dependent constant and $\varepsilon_0$ of 0.2 to 0.4 is a critical strain where sub-boundaries are produced by lattice rotations through accommodation slips. Thus, the progress in continuous dynamic recrystallization can be illustrated by increasing the fraction of high-angle boundaries (Figure 5) [41]. In a coarse-grained ferritic steel, the sharp maximum corresponding to low-angle dislocation sub-boundaries evolved at early deformation decreased and spread out toward high-angle misorientations with straining (Figure 5a). After large strains, the deformation boundaries/sub-boundaries are characterized by flat-type misorientation distributions with almost equal fractions of different misorientations. It should be noted that the misorientation distribution in the initial martensitic microstructure containing a rather large fraction of high-angle boundaries resulted from the phase transformation changed in similar way (Figure 5b). Namely, both low-angle and high-angle maximums were weakened by the plastic working, leading to a flat-type misorientation distribution after deformation to sufficiently large strains. It is interesting that further deformation resulted in an increase in the fraction of high-angle boundaries with misorientations above 50°. Flat-type misorientation distributions with two little maximums against small angles below 15°, and large angles above 50° were frequently observed in the severely strained metals and alloys [41,51,56,65–67].

A special role in the development of high-angle grain boundaries of deformation origin belongs to geometrically necessary sub-boundaries separating the portions of original grains, where operating slip systems are different [68]. The misorientations across such sub-boundaries rapidly increase up to typical values of ordinary high-angle grain boundaries during deformation. The microshear bands involving local strain gradient are rich in the geometrically necessary boundaries and may be considered as preferential nucleation sites for the strain-induced ultrafine grains. Figure 6 shows typical deformation microstructures evolved in a 316L-type austenitic stainless steel during warm rolling [55]. It is clearly seen that the fraction of ultrafine grains significantly increases during deformation owing to increasing density of microshear bands (MSB in Figure 6).

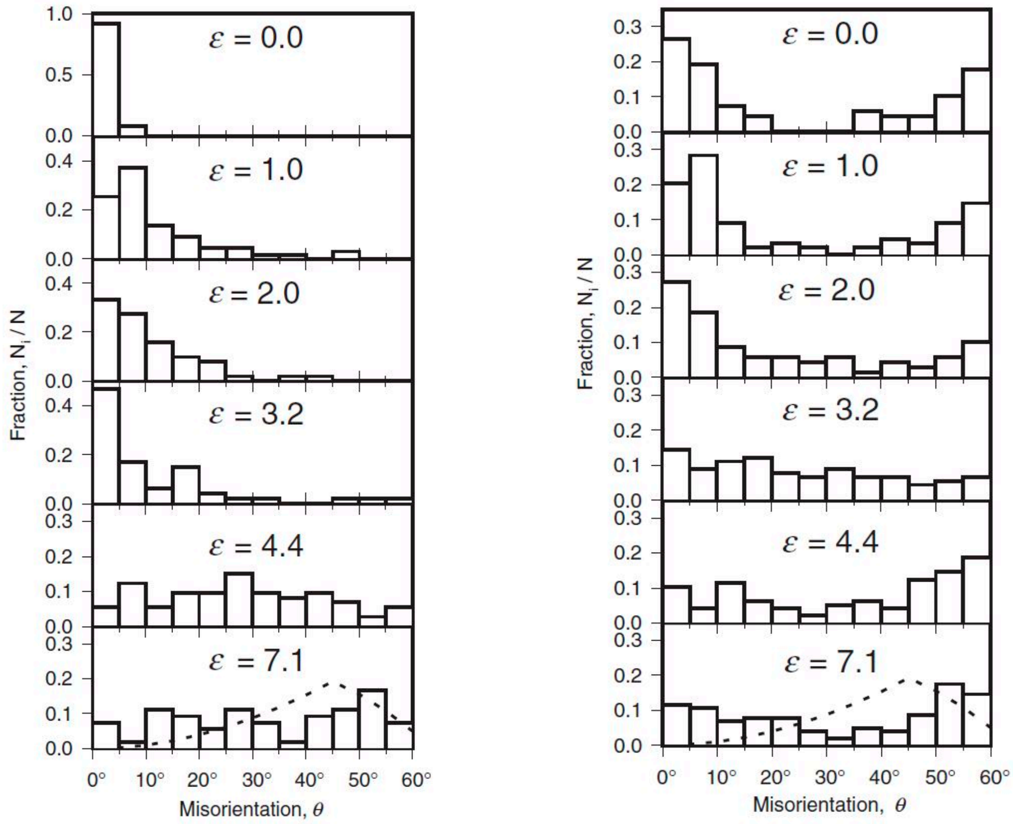


(**a**) (**b**)

**Figure 5.** Misorientation distribution for the grain/subgrain boundaries evolved in an Fe-22%Cr-3%Ni steel (**a**) and an Fe-18%Cr-7%Ni steel (**b**) subjected to cold bar rolling/swaging to various total strains [41].

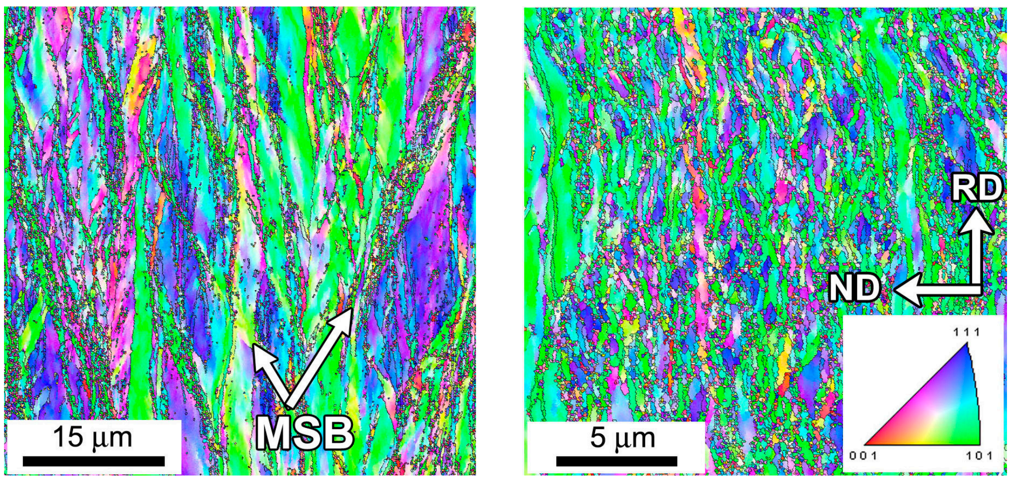


(**a**) (**b**)

**Figure 6.** Deformation microstructures in a 316L-type austenitic stainless steel subjected to warm rolling at 573 K to total strain of 2 (**a**) and 3 (**b**) [55]. The inverse pole figures are shown for the normal direction (ND).

*3.1. Grain Size*

The grain subdivision by the geometrically necessary boundaries during cold-to-warm working should gradually decrease the grain size, finally leading to the ultrafine grained microstructure. In the case of unidirectional deformation, the transverse grain size should also be reduced following the change in the whole sample geometry. The strain effect on the transverse grain/subgrain size in a two-phase austenite–ferrite stainless steel subjected to cold bar rolling, followed by swaging is shown in Figure 7a [69]. The change in the phase dimensions crosswise to the rolling/swaging direction is also shown in Figure 7a. It is clearly seen that the phase dimensions correspond well to the change of the sample shape in the strain range with constant phase content (solid line range in Figure 7a). This correlation testifies to uniform deformation across the sample. In contrast, the transverse grain/subgrain size decreases much faster than that of the whole sample in the range of relatively small total strains. Then, the strain dependence of the transverse grain/subgrain size weakens with straining that leads to apparent steady-state behavior when the transverse grain/subgrain size becomes strain invariant in large strains. Note that strain-induced martensitic transformation (dashed line range in Figure 7a) does not affect the general grain size–strain dependence. Therefore, the region of small strains corresponds to the grain refinement that is associated with the development of new strain-induced grain boundaries (Figure 7b) [53]. On the other hand, the number of grains/subgrains on the cross-section of the sample decreases in the range of large total strains. Such an apparent increase in the grain size can be attributed to the pronounced microshearing accompanied with a kind of grain/subgrain coalescence, e.g., boundary merging by Y-joint motion [53,69–71], resulting in the apparent steady-state deformation behavior (Figure 7b). Similar strain dependence of the grain size is commonly observed in various quasi-single phase metals/alloys irrespective of material type and processing method [5,14,15,39,41,69].

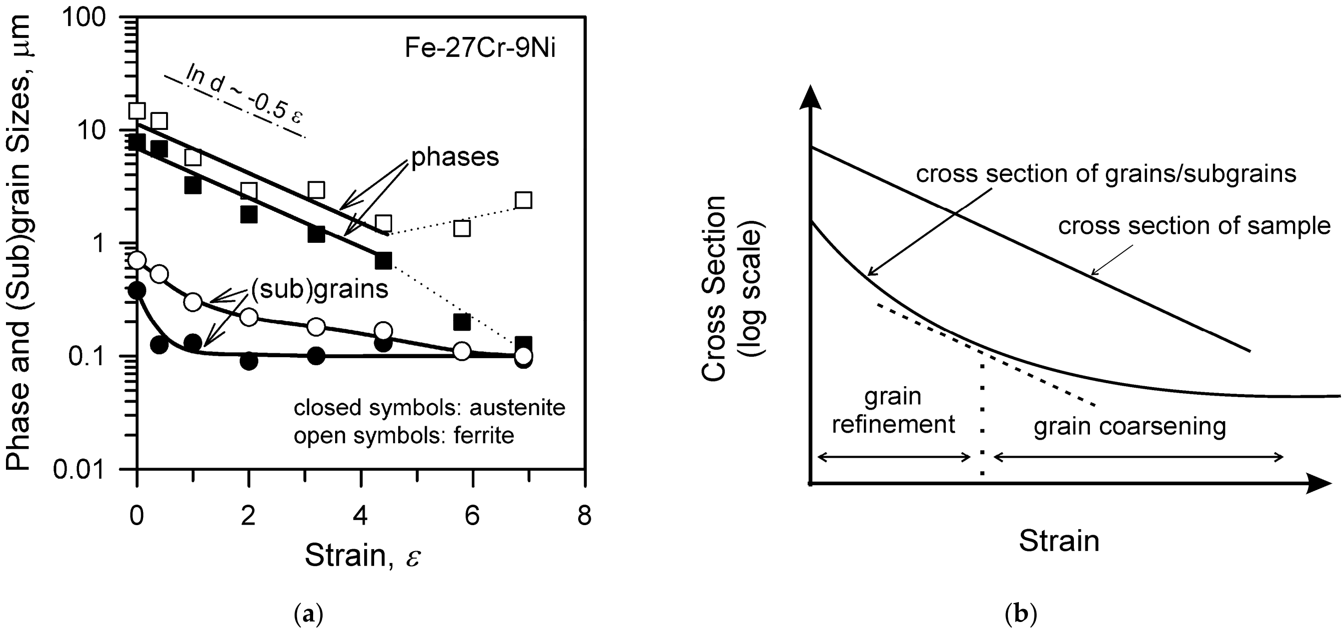


**Figure 7.** Strain effect on the transverse size (**a**) and the cross-section (**b**) of grains/subgrains, phases, and sample during bar rolling/swaging [53,69].

The fine-grained microstructures evolved by severe deformation were considered to result from the progressive transformation of the strain-induced subgrains [15]. The transformation involves a gradual increase in misorientations between the deformation subgrains owing to accumulation of geometrically necessary dislocations caused by some local strain gradients and/or local strain incompatibilities. The grain refinement was modeled by Toth et al. based on the lattice curvature that develops in all deformed grains [72].

The lattice rotations within a deformed grain were assumed to be non-uniform because of the constraining effect of the neighboring grains. Hence, the orientation gradients develop in the original grains toward the grain boundaries during deformation. Then, the geometrically necessary dislocations are accumulated to accommodate this evolving curvature and build up a new strain-induced boundary. This model corresponds to experimental observations of the progress in the strain-induced grain development, which starts from original grain boundaries [24,25], and it explains the effect of original grain size on the kinetics of grain refinement during cold-to-warm working [73], although the effect of microshear bands on heterogeneous formation of new grains is neglected.

Taking into account heterogeneous formation of strain-induced ultrafine grains with a size of $D_{UFG}$ in a microstructure with an initial grain size of $D_0$ upon severe plastic deformation, Morozova and Kaibyshev expressed the mean grain size during the grain refinement process as follows [74]:

$$D_\varepsilon = ((1 - F_{UFG})D_0{}^{-2} + F_{UFG}D_{UFG}{}^{-2})^{-0.5} \tag{4}$$

Substituting the fraction of ultrafine grains, $F_{UFG} = 1 - \exp(-k\varepsilon^n)$, where k and b are constants, and ignoring $(D_{UFG}/D_0)^2$ because $D_{UFG} << D_0$, we see that the mean grain size reads as follows:

$$D_\varepsilon = D_{UFG}(1 - \exp(-k\varepsilon^n))^{-0.5} \tag{5}$$

In spite of apparent simplicity, Equation (5) provides fairly good agreement with experimental data for various materials (Figure 8) [74,75]. Note here that Equation (5) well predicts the mean grain size even in metastable austenitic steels experiencing partial martensitic transformation during cold deformation (304L in Figure 8a), because the grain refinement due to the transformation can be discussed with the same speculation leading to Equation (4).

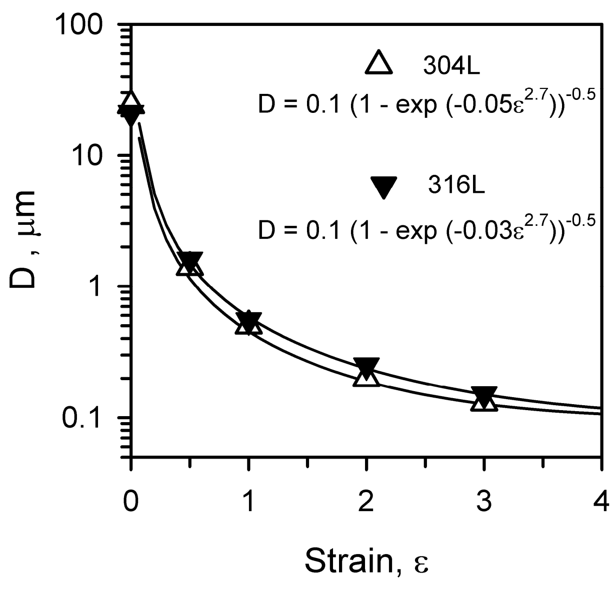


(**a**)

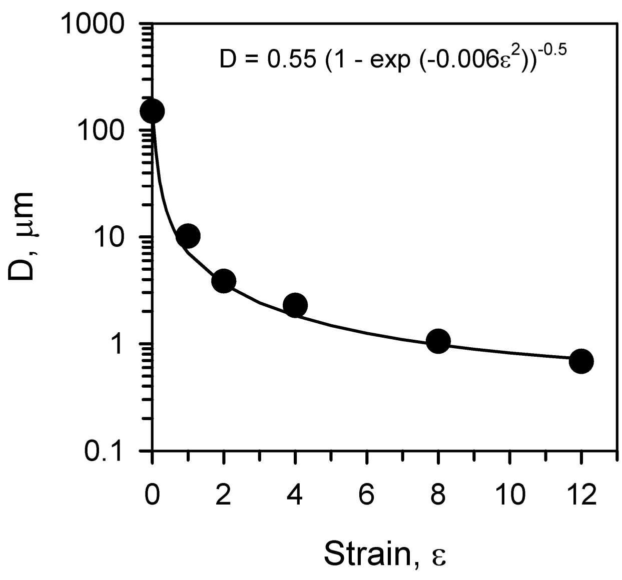


(**b**)

**Figure 8.** Reduction of an average grain size in stainless steels [75] (**a**) and a copper alloy (**b**) during cold rolling [74].

The final grain size, which can be attained in metallic materials by large strain deformation, depends on processing conditions and can be related to the flow stress through a power-law function. A power-law function between the grain size and the flow stress was frequently observed in dynamic recrystallization (DRX) under hot-working conditions [57]. An exponent in the relationship between the flow stress and the grain size depends on the processing conditions, which dictate the operating mechanisms for the microstructure evolution [57,76–80]. Generally, three domains can be distinguished, especially in fcc-metals/alloys with low-to-medium SFE experiencing discontinuous DRX during hot deformation (Figure 9). In the range of low flow stress, i.e., under hot-deformation conditions, the dynamic grain size can be expressed by a power-law function of flow stress with a grain size exponent of about −0.7. Such values were frequently observed in hot-worked microstructures that resulted from discontinuous DRX consisting of cyclic nucleation and growth of new grains [9–11]. Under conditions of cold working with high flow stress, the size of the ultrafine grains developed by the grain subdivision mechanism during severe deformation tends to approach the size of deformation subgrains [78–80]. Note that data points shown in the high-stress domain in Figure 9 correspond to deformation grain size unaffected by phase transformations. Thus, an exponent of about −1.0 was reported for various metallic materials [81], as can be expected from the Taylor-type relationship [82]. In the range of intermediate flow stress between cold and hot deformation, i.e., under warm-working condition, the new fine grains evolve by means of continuous DRX. Therefore, the grain-boundary migration and the grain growth critically depend on the deformation temperature, resulting in an exponent of about −0.3 [57].

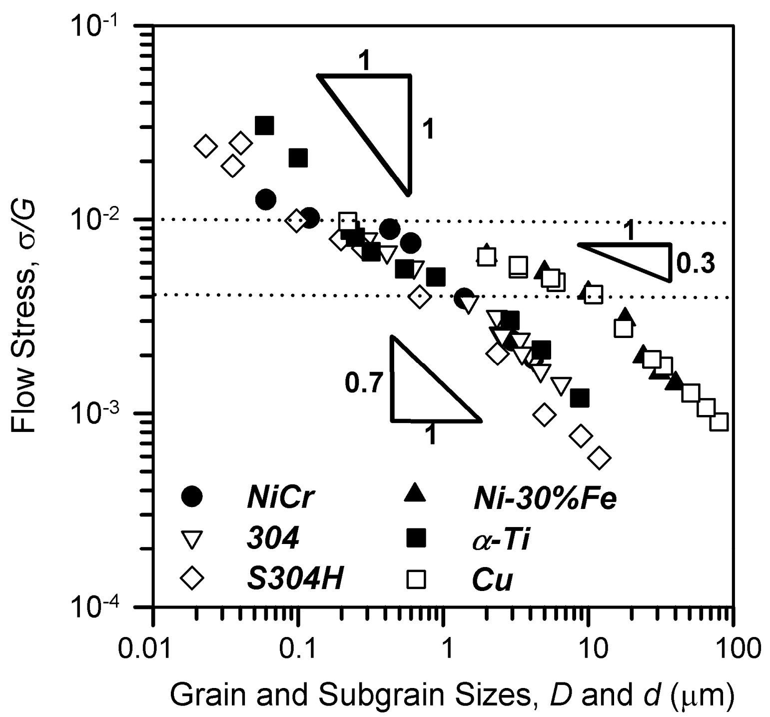


**Figure 9.** Relationship between the flow stress and the grain/subgrain size evolved during large strain deformation under cold-to-hot working conditions [25,73,76–79].

*3.2. Dislocation Density*

The straining of metallic materials under conditions of cold-to-warm deformation is commonly accompanied by an increase in dislocation density [82–84]. Mecking and Kocks succeeded in the modeling of deformation behavior, relating the flow stress to the evolution of the dislocation density [85]. The change in the dislocation density during deformation was considered as a result of two concurrent processes [85,86].

$$D\rho/d\varepsilon = h - r\,\rho \tag{6}$$

where the first term represents athermal dislocation storage, i.e., $h = (b\Lambda)^{-1}$, where b and $\Lambda$ are the Burgers vector and a mean free path, respectively; and the second one with a parameter of r is dependent on deformation conditions, i.e., temperature and strain rate, corresponds to decreasing the dislocation density by means of dynamic recovery. Setting initial dislocation density of $\rho_0$ at $\varepsilon = 0$, Jonas et al. obtained the following expression for the dislocation density [87].

$$\rho = (h - (h - \rho_0 r) \exp(-r\varepsilon))/r \tag{7}$$

The strain dependence of the dislocation density in the form of Equation (7) predicts a gradual decrease in the rate of dislocation accumulation during deformation. Taking $\rho_0 << \rho$ and r = 1 for simplicity, the strain effect on the evolution of the dislocation density in various metallic materials is displayed in Figure 10. The symbols in Figure 10 indicate the experimental values of dislocation density obtained by either direct counting the individual dislocations in grain/subgrain interiors, using transmission electron microscopy (TEM) [55,75,88] or evaluated by orientation imaging microscopy (OIM) [74,88] with automatic analysis of electron backscattered diffraction (EBSD) patterns. The lines in Figure 10 correspond to approximation by Equation (7). Following the rapid increase in the dislocation density at early deformation, the dislocation density tends to approach an apparent saturation at sufficiently large strains irrespective of possible phase transformation, e.g., partial martensitic transformation in 304L steel at 473 K in Figure 10a. Therefore, a steady-state deformation behavior, when neither the grain size nor the dislocation density varies with strain, can be attained during deformation even at relatively low temperatures.

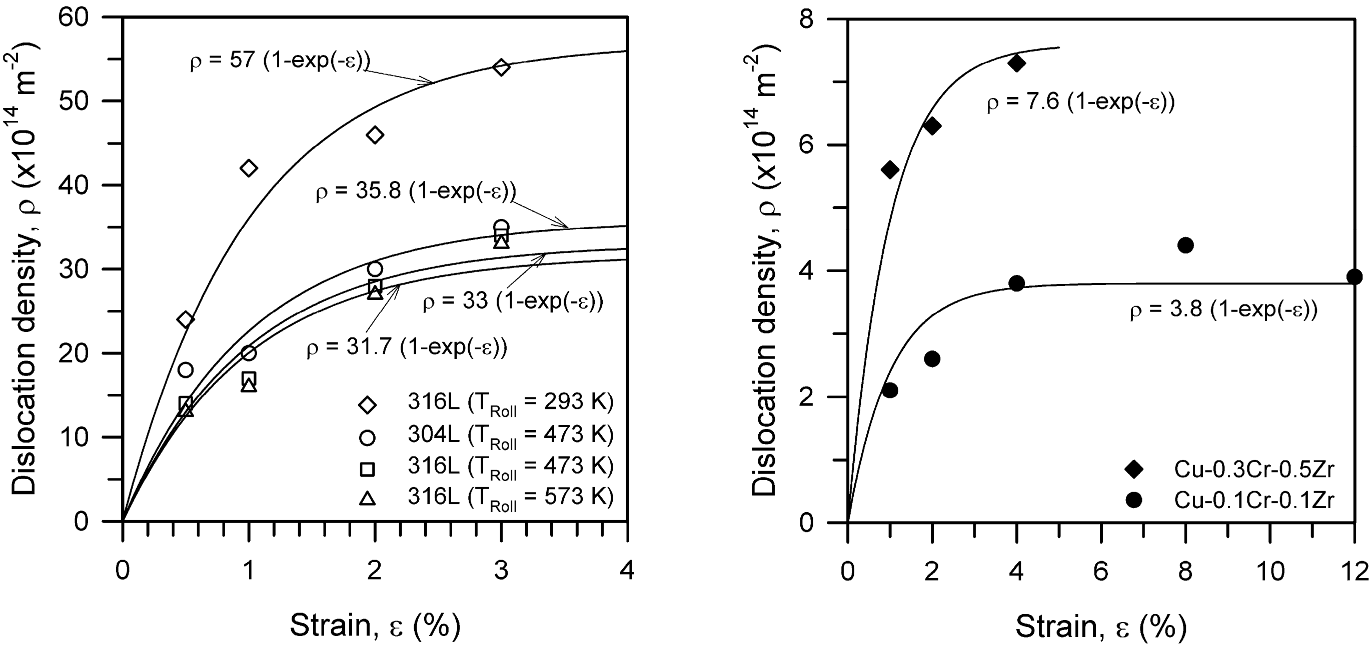


(**a**) (**b**)

**Figure 10.** Strain effect on the dislocation density in various steels [55,75] (**a**) and copper alloys [74,88] (**b**) subjected to large strain deformation.

The dislocation density in ultrafine grains that evolved by severe deformation reportedly tended to decrease upon further straining, while residual stresses continued accumulation [24,41]. The high internal stresses in severely strained metallic materials were attributed to strain-induced grain boundaries being in non-equilibrium state [15,89–91]. An irregular increase in the density of geometrically necessary dislocations at strain-induced grain boundaries creates large lattice distortions along such non-equilibrium boundaries. The largest distortions are expected at grain boundary junctions that lead to the development of junction disclinations bearing long-range internal stresses [64,90–94]. The latter ones were discussed being responsible for an apparent decrease in the dislocation density within the strain-induced ultrafine grains [24,25,41].

The strain dependencies for the grain size and the dislocation density (Equations (5) and (7)) predict a power-law function between the microstructural parameters, i.e., the deformation grain size and dislocation density. Figure 11 shows the relationship between the grain size (the transverse grain size in the case of unidirectional straining) that developed at various deformation stages and the corresponding dislocation density evolved in these grains/subgrains [75,88,95–99]. It is clearly seen in Figure 11 that a linear function with a slope of −2 generally holds between the grain size and the dislocation density plotted in double log scale. It should be noted that the grain size and dislocation density plotted in Figure 11 correspond to deformation microstructures evolved in a wide range of total strains from early to severe deformation. Moreover, the range of deformation conditions in Figure 11 spans from cold deformation with a partial martensitic transformation in 304L steel to hot working, which was accompanied by discontinuous DRX in the selected materials. Hence, the revealed unique relationship reflects the intimate linkage among the microstructural parameters of various metals and alloys subjected to plastic deformation.

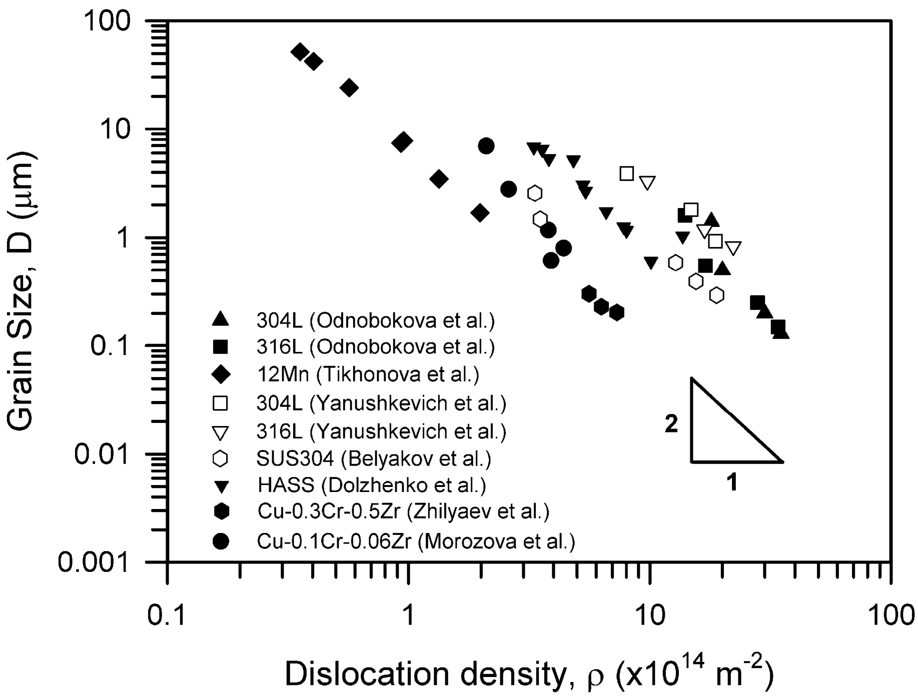


**Figure 11.** Relationship between the grain size and dislocation density in various steels, including AISI stainless steels, high-manganese steel (12Mn), highly alloyed austenitic stain less steel (HASS), and copper alloys processed by cold-to-hot working [75,88,95–99].

### 3.3. Varying the Strain Path

The effect of processing regimes on the microstructure evolution in various metallic materials subjected to large strain deformation has been a subject of numerous research studies [15,33,100–103]. It is generally agreed that the finally achievable grain size evolved at sufficiently large strains sensitively depends on deformation temperature and strain rate. In contrast, the deformation method has a marginal effect on the final grain boundary spacing, although it can significantly affect the shape of strain-induced grains [51]. On the other hand, the kinetics of the microstructure evolution may substantially vary depending on the processing method. The effect of varying strain path on the grain refinement kinetics during cold-to-warm working is still debatable. The change in the strain paths from pass to pass during multiple deformations was frequently considered to be very important for the formation of ultrafine grains [14,24,25,104]. Alternatively, the unidirectional deformation was also discussed to promote the microstructure evolution kinetics, especially at elevated temperatures [101,102].

Applying the different rotations of the ECAP samples between each pressing pass, the effect of change in the shear plane on the microstructure evolution was studied in pure aluminum at room temperature [105]. The most rapid increase in misorientations between deformation subgrains was observed in the ECAP samples rotated by 90° around its axis, when the shear planes intersected at 120° and the subgrain bands developed on two separate intersecting planes (route B in Figure 12). In contrast, the slowest grain refinement kinetics was demonstrated by the ECAP samples without rotation, when the shearing was accumulated monotonously along two orthogonal planes (route A in Figure 12). Note here that the evolution kinetics was studied by the diffraction spot spreading, which gave no way of deducing any quantitative relations.

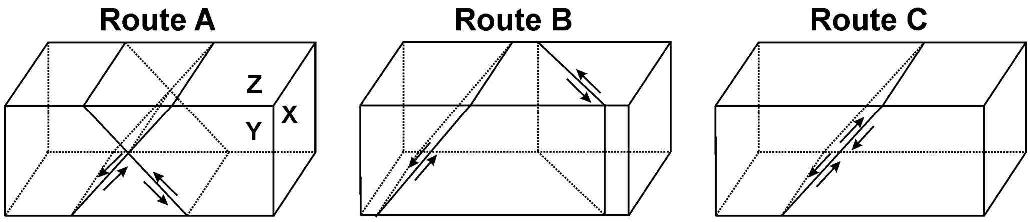


**Figure 12.** Shearing patterns during subsequent ECAP with different strain paths [105].

The most significant effect of varying the strain path on the deformation microstructure evolution could be expected in comparison of unidirectional and multidirectional processing. At relatively small total strains, however, the deformation microstructures consisting of dislocation cell blocks in bcc-steel were almost the same irrespective of processing method at room temperature (Figure 13a,c) [51]. A remarkable difference in the deformation microstructures evolved by either unidirectional bar rolling/swaging or multidirectional forging was observed after relatively large strains [51]. Highly elongated grains were developed during unidirectional deformation, whereas multidirectional deformation promoted the development of almost equiaxed grains (Figure 13b,d). It is interesting that the transverse grain/subgrain size could be represented by a unique function of total strain for both processing methods (Figure 14a). Similarly, the fraction of high-angle boundaries increased almost linearly with straining to total strains of about 4 irrespective of difference in deformation techniques and, then, tended to saturate at 0.8 or 0.6 for rolling/swaging or multiple forging, respectively (Figure 14b). This difference in a ratio of strain-induced high-angle grain boundaries to low-angle sub-boundaries was attributed to strong fiber texture leading to accumulation of large misorientations around 60° in the rolled/swaged samples [53].

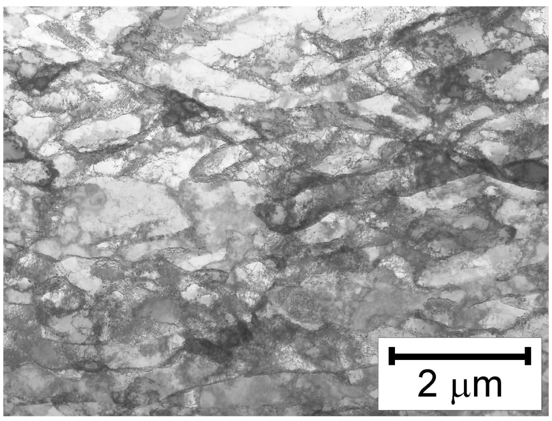


(**a**)

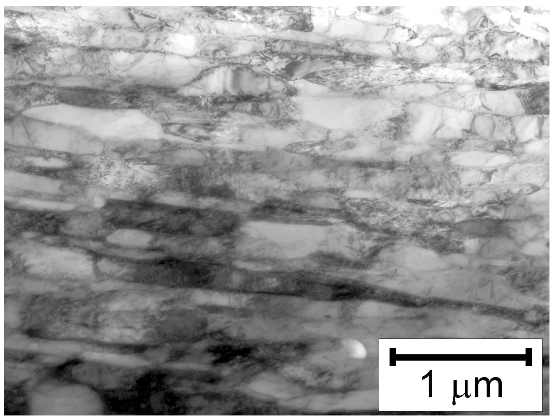


(**b**)

**Figure 13.** *Cont.*

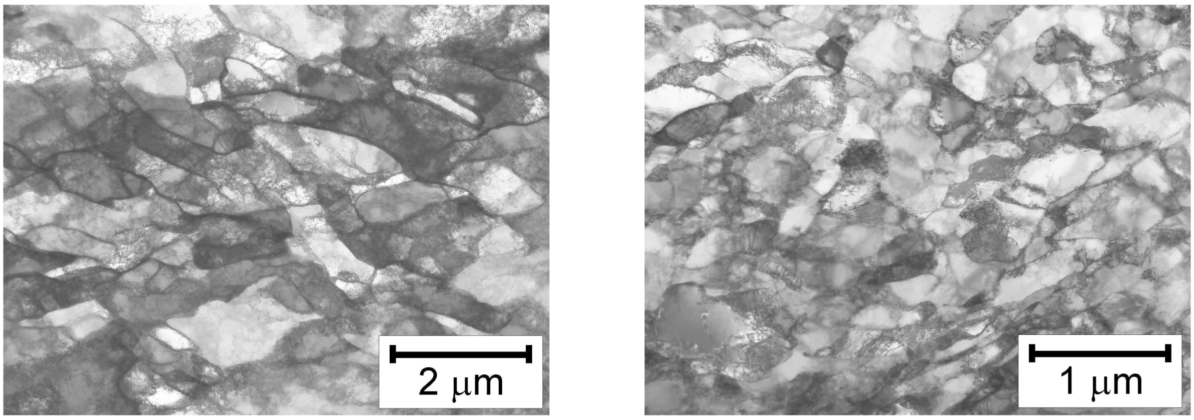


(**c**) (**d**)

**Figure 13.** Deformation substructures developed in an Fe-15%Cr ferritic stainless steel during bar rolling/swaging to total strain of 1.0 (**a**) or 7.2 (**b**), or during multiple forging to total strain of 0.8 (**c**) or 7.2 (**d**) [51].

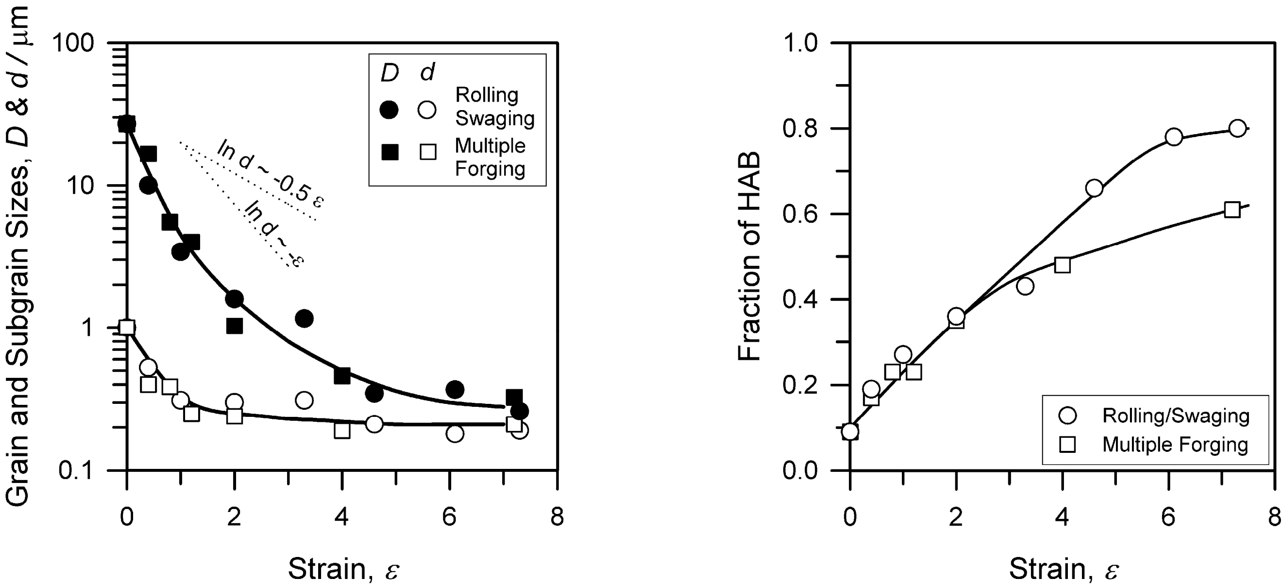


(**a**) (**b**)

**Figure 14.** Effect of processing method on the transverse grain/subgrain size (**a**) and the fraction of strain-induced high-angle grain boundaries (**b**) in an Fe-15%Cr ferritic stainless steel [53].

### *3.4. Temperature Effect*

The deformation temperature significantly affects both the strain-induced grain size and the kinetics of microstructure evolution. Decreasing the deformation temperature results in a decrease in the mean grain size evolved at large strains under conditions of warm-to-hot working (Figure 15) [106]. The new grains rapidly develop during hot deformation, owing to discontinuous DRX (annealing twins in Figure 15 are indicative of this DRX mechanism). The grain refinement with a decrease in deformation temperature is accompanied by slowing down the kinetics of new grain development. The new grains resulted from continuous DRX primarily develop along the original grain boundaries and microshear bands, resulting in a necklace-like microstructure under conditions of warm working (Figure 15).

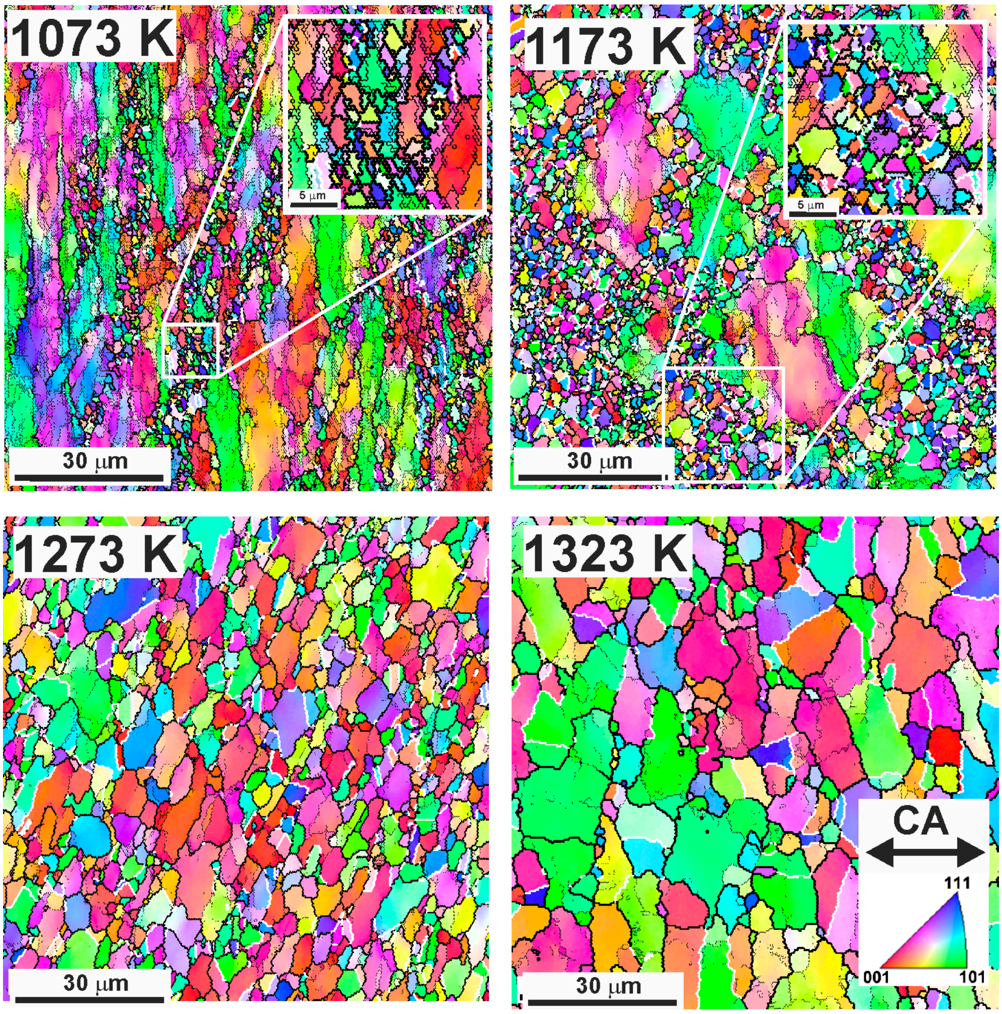


**Figure 15.** Typical deformation microstructures evolved in an austenitic stainless steel subjected to isothermal compression to a strain of 1.2 at indicated temperatures [106]. The gray and black lines correspond to the subgrain and grain boundaries, respectively. The white lines indicate the annealing twins. The colors reflect the inverse pole figures for the compression axis (CA).

Generally, a power-law function holds between the temperature-compensated strain rate (or Zener–Hollomon parameter) and the dynamic grain size (Figure 16) [10,103,107–111]. A strain-rate exponent of about −0.4 in the range of hot deformation, which is accompanied by discontinuous DRX, changes to about −0.1 in continuous DRX with a decrease in temperature down to cold deformation. Such relationships can be derived by combining the power-law functions between the flow stress and the deformation grain size (Figure 9) with those between the flow stress and the temperature-compensated strain rate [9,112–114].

An increase in deformation temperature from cold-to-warm working leads commonly to more homogeneous dislocation substructures. Cold working of metals and alloys is frequently accompanied by strain localization in deformation microbands, shear bands, S-bands, etc. [57,115]. In contrast, uniform dislocation subgrains resulted from dynamic recovery develop in various metallic materials during hot working [9,57]. Warm working is an intermediate domain, where the extent of strain localization depends on deformation mechanisms, including the variety of active slip systems, dislocation ability to dynamic recovery, strain hardening, etc. An example of the deformation microstructures evolved in a high-strength low-alloyed steel during warm rolling is shown in Figure 17 [111]. The transverse grain size in these recovery-controlled microstructures exhibits rather strong dependence on the deformation conditions with a strain rate exponent of −0.3 [111] that corresponds to the transition domain between hot and cold deformation in Figure 16.

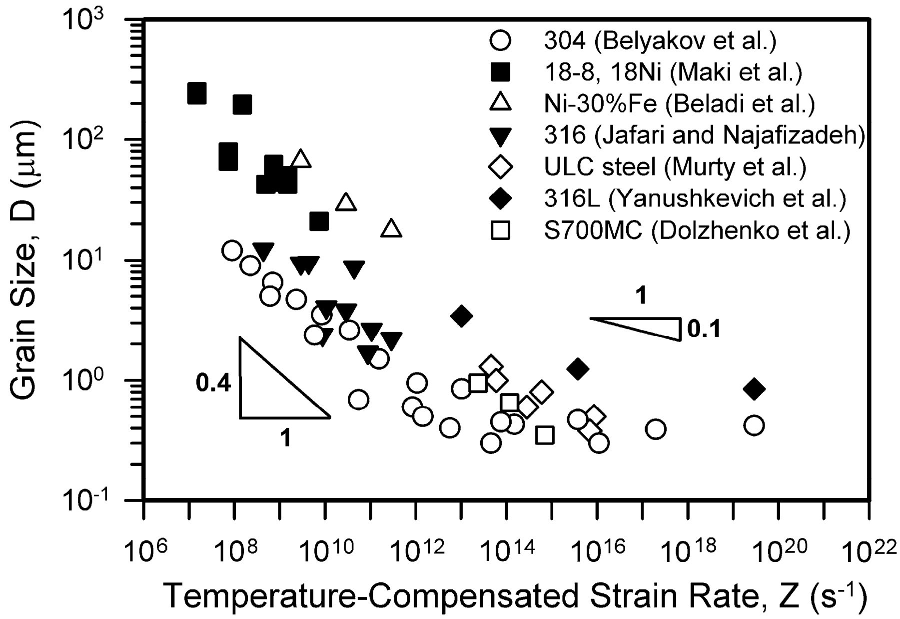


**Figure 16.** Effect of deformation conditions on the grain size evolved in large strains in various fcc-alloys, such as AISI stainless steels, maraging steel (18Ni), nickel-chromium alloy (Ni-30%Cr), and bcc-alloys, namely, ultralow carbon (ULC) and high-strength low-alloyed (S700MC) steels [10,103,107–111].

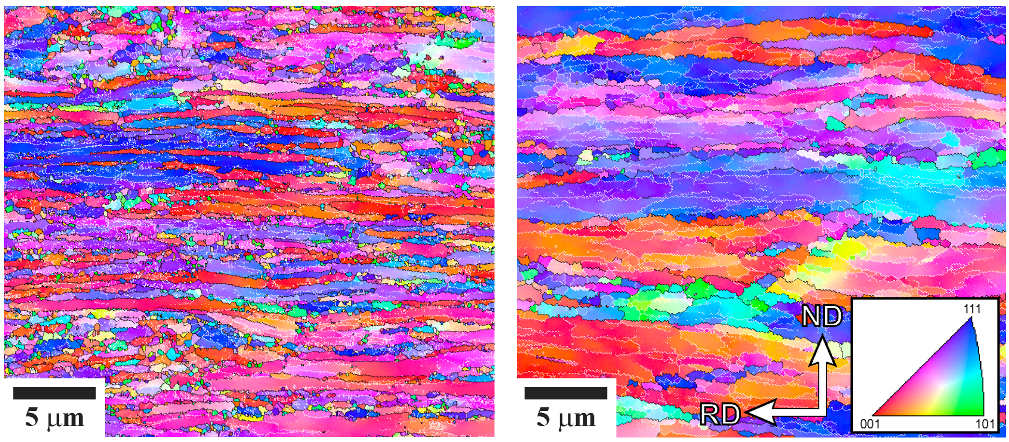


(**a**) (**b**)

**Figure 17.** Deformation microstructures evolved in a high-strength low-alloy steel after warm rolling to a total strain of 1.5 at 923 K (**a**) or 973 K (**b**) [111]. Colors indicate the direction along the normal direction (ND).

In the case of strong temperature and/or strain dependence of deformation mechanisms, such as slip/twinning in hcp-metallic materials, unusual temperature/strain dependence of the grain size can be observed during transient deformation stage [62,63]. The change in the contribution of deformation twinning to the new grain development in Mg during cold deformation reportedly led to an apparent increase in the dynamic grain size during straining to moderate strains. Nevertheless, further severe deformation was accompanied by a gradual grain refinement leading to common steady-state deformation behavior [63].

An increase in deformation temperature promotes dynamic recovery, which, in turn, assists the development of new grains owing to continuous DRX [57,66]. An average misorientation of strain-induced grain boundaries can be expressed by a linear function of total strain similar to maximal misorientation in Equation (3). The rate of the misorientation increase reportedly increases with deformation temperature. The development of strain-induced grain boundaries was accelerated in pure copper subjected to multiple forging with increasing the deformation temperature from 195 K to 473 K, especially in large total strains above 2 (Figure 18a) [116]. Similar effect of deformation temperature on the rate of misorientation increase for the strain-induced grain boundaries was observed by Tsuzaki et al. in stainless steel, when the misorientation rates of 4° and 12° were obtained for cold-rolling with annealing and hot-rolling with annealing, respectively [117]. High values of the misorientation rate up to 40° were reported for continuous DRX of aluminum alloys during hot working under superplastic conditions [118]. On the other hand, an increase in the fraction of strain-induced grain boundaries was almost temperature independent in a 304-type stainless steel during warm rolling at 773 to 1273 K (Figure 18b) [119]. In this case, almost the same kinetics for the development of strain-induced grain boundaries at different rolling temperatures was discussed as a result of microstructure evolution due to simultaneous operation of two different mechanisms. One of them is the recovery-controlled grain boundary formation, and the second one is the microband assisted grain development. The former is accelerated by temperature, whereas the latter is stunted by temperature. Hence, the opposite temperature effect on the contribution of these mechanisms led to temperature-independent kinetics of strain-induced grain boundary formation in a wide range of warm working.

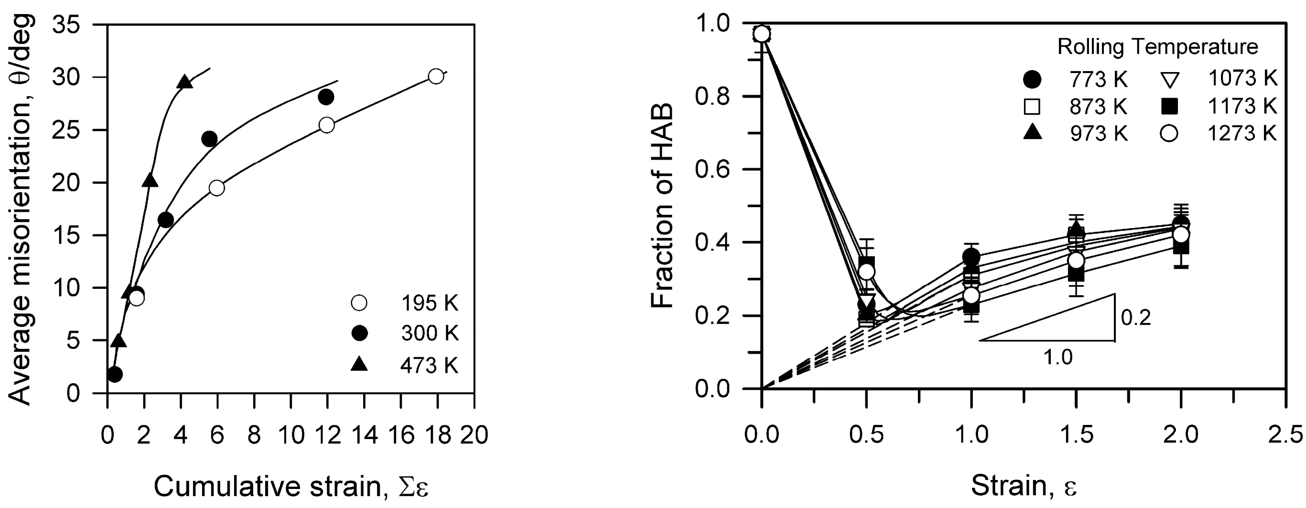


(**a**) (**b**)

**Figure 18.** Effect of deformation temperature on the grain/subgrain boundary misorientations in pure copper subjected to multiple forging (**a**) [116] and the fraction of high-angle grain boundaries (HAB) in an S304H-type stainless steel subjected to bar rolling (**b**) [119].

Slowing down the kinetics of strain-induced grain boundary development with an increase in deformation temperature was observed in an aluminum alloy subjected to ECAP [102,120]. The deformation microbanding assisted by high-density precipitate particles was considered as crucial factor for the strain-induced grain evolution in materials with high SFE. Metals and alloys that are highly prone to dynamic recovery are characterized by homogeneous dislocation substructures developed at elevated deformation temperatures that hardly transform to the new grains even at large strains. The grain refinement in such materials during warm-to-hot working was attributed to geometric DRX, which readily occurs after sufficiently large strains under conditions of constant strain path [121].

## 4. Deformation Texture

The deformation microstructures are scarcely affected by discontinuous DRX under conditions of cold-to-warm working at relatively low temperatures [57]. Correspondingly, the texture developed depends on the operating deformation mechanisms, i.e., slip systems in conventional ductile metals and alloys, which, in turn, are governed by crystal symmetry [5]. Thus, the deformation texture is determined by processing method. Widely used technologies involving caliber or plate rolling should lead to strong deformation texture depending on the total strain of unidirectional deformation. On the other hand, severe plastic straining is frequently based on redundant deformations involving regular alternating strain path, such as multiple forging. Thus, the textures developed in metallic materials subjected to multiple straining applications depend significantly on the strain in the last deformation pass, when the deformed material experiences the final reorientation. In contrast to previous sections that dealt with general regularities of the deformation microstructure evolution inherent to various metallic materials without clear separation into different lattices, the textural changes are outlined sequentially for specific crystals.

### *4.1. Conventional Processing*

The development of deformation texture in fcc-metals and alloys depends on deformation mechanisms, which, in turn, depend on alloying extent, dispersed precipitations, and SFE [5,56,122–126]. The effect of solid solution and dispersion strengthening on the deformation texture is illustrated in Figure 19, which shows pole figures for {111}, {200}, and {220} planes in a pure cupper and a Cu-Ni-P alloy observed after cold rolling to a total strain of 5 [56]. Pure Cu displays typical copper-type rolling texture, while the copper alloy after solution treatment (ST) and that containing finely dispersed particles after ST followed by low temperature aging (400 °C) resemble brass-type textures as clearly seen in the {200} pole figures. On the other hand, the alloy with relatively large particles after ST followed by high temperature aging (600 °C) demonstrates a texture of mixed type, which shows the features inherent to both the copper-type and brass-type textures. The brass-type texture evolution was attributed to the extensive development of microshear bands in the alloys after solution treatment and low temperature aging. The microshearing in the alloy after high temperature aging was delayed and took place after rather large strains following uniform deformation substructures similar to those in pure copper, resulting in the mixed deformation texture.

The rolling textures in fcc-metals/alloys can be represented by evolution of three main components, i.e., {112}<111> (copper orientation), {011}<211> (brass orientation), and {123}<634> (S orientation) [122,123]. Ideal texture orientations are shown on the section of orientation distribution functions (ODF) in Figure 20 and listed in Tables 1 and 2 [127]. A decrease of SFE promotes the development of deformation twinning, followed by shear banding, and, therefore, leads to reduction of the intensity of the copper texture, whereas the fraction of brass texture increases [123,125]. The texture evolution in a high-Mn steel with low SFE subjected to cold rolling was characterized by a rapid development of strong brass and S components, and a copper-twin component, which strengthened with straining because of frequent deformation twinning (Figure 21) [128]. At large rolling strains the deformation twinning exhausted and the microshear banding promoted the E and F textures located on the $\gamma$-fiber. A gradual increase of the fractions of copper-twin and Goss textures at large strains in Figure 21 was attributed to dislocation slip in microshear bands and twin/matrix lamellae [128]. Simultaneous development of the brass, copper-twin, and Goss textures could be responsible for the texture maximum located on the $\zeta$-fiber. SFE decreases with an increase in temperature. Therefore, characteristic rolling textures tend to weaken with increasing deformation temperature [98].

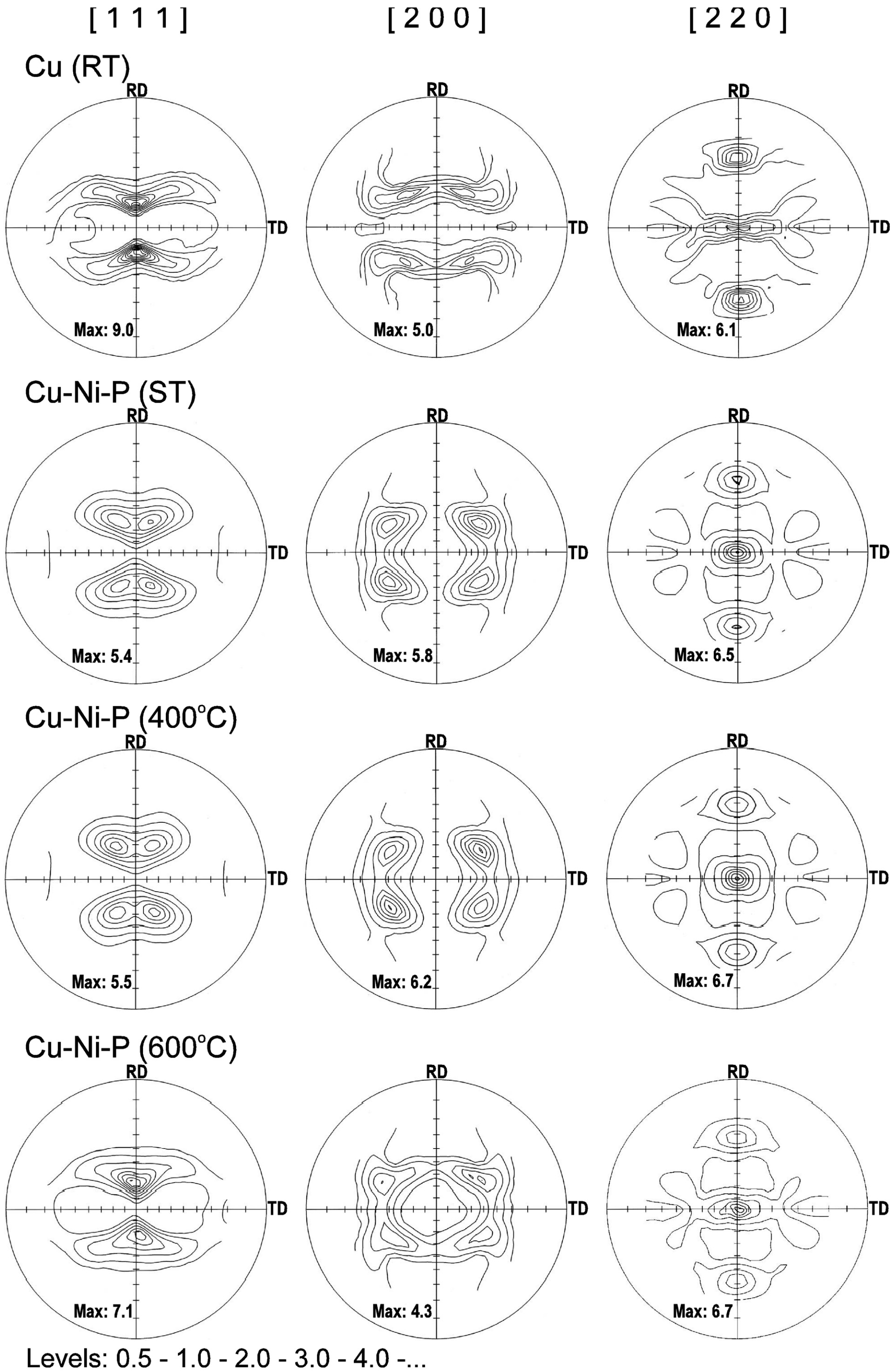


**Figure 19.** Characteristic pole figures evolved by cold rolling to a strain of 5.0 in a pure copper and a Cu-1.5%Ni-0.3%P alloy after solution treatment (ST), or solution treatment and aging at 673 K (400 °C), or solution treatment and aging at 873 K (600 °C) [56].

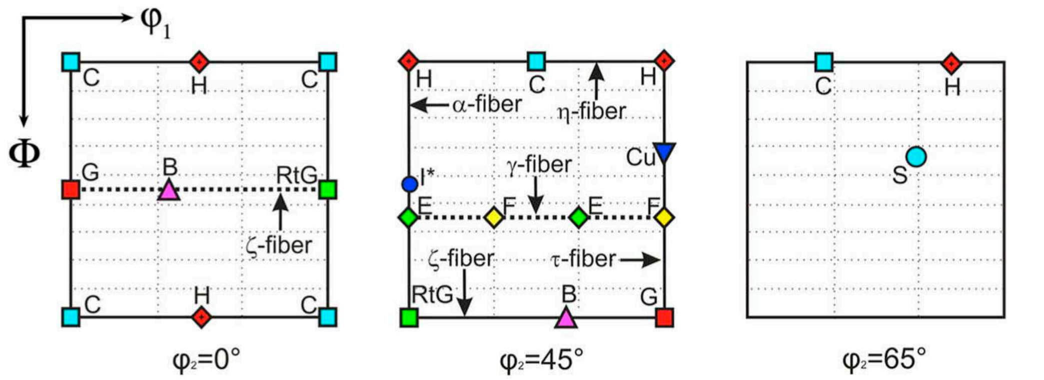


**Figure 20.** Some specific textures on the corresponding sections of orientation distribution functions [127].

**Table 1.** Definition of characteristic texture components in fcc-metals [125].

| Component | {hkl} <uvw> | Euler Angles | | |
|---|---|---|---|---|
| | | $\varphi_1$ | $\Phi$ | $\varphi_2$ |
| Brass (B) | {111}<112> | 55 | 90 | 45 |
| Goss (G) | {011}<100> | 90 | 90 | 45 |
| S | {123}<634> | 59 | 37 | 63 |
| Copper (Cu) | {112}<111> | 90 | 35 | 45 |
| Rotated Goss (RtG) | {011}<110> | 0 | 90 | 45 |
| E | {111}<110> | 0/60 | 55 | 45 |
| F | {111}<211> | 30/90 | 55 | 45 |
| ζ-fiber | <110> parallel to ND | | | |
| γ-fiber | <111> parallel to ND | | | |
| τ-fiber | <110> parallel to TD | | | |

**Table 2.** Definition of characteristic texture components in bcc-metals [127].

| Component | {hkl} <uvw> | Euler Angles | | |
|---|---|---|---|---|
| | | $\varphi_1$ | $\Phi$ | $\varphi_2$ |
| Cube (C) | {001}<100> | 45 | 0 | 45 |
| Rotated cube (H) | {001}<110> | 0/90 | 0 | 45 |
| I* | {223}<110> | 0 | 43 | 45 |
| E | {111}<110> | 0/60 | 55 | 45 |
| F | {111}<211> | 30/90 | 55 | 45 |
| Goss (G) | {110}<001> | 90 | 90 | 45 |
| η-fiber | <001> parallel to ND | | | |
| α-fiber | <110> parallel to RD | | | |
| γ-fiber | <111> parallel to ND | | | |

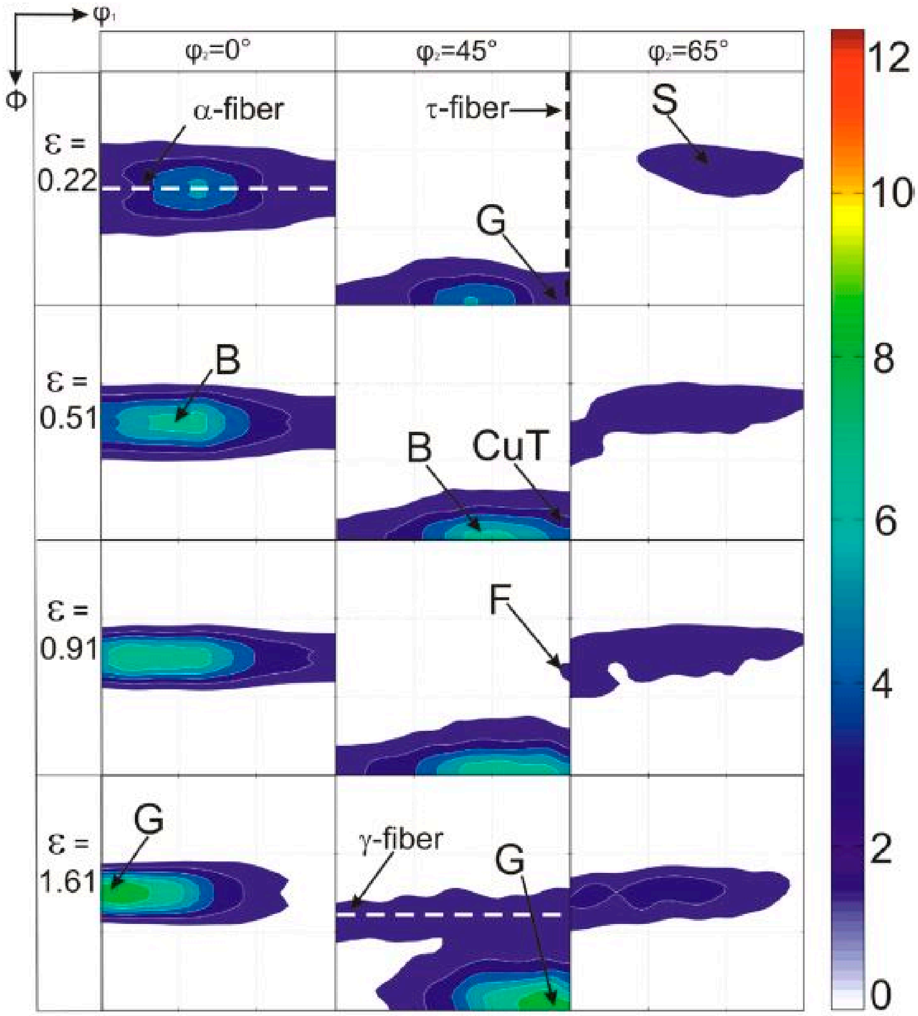


**Figure 21.** Effect of cold rolling on the textures in an Fe-17%Mn-1.5%Al-0.3%C steel [128].

The rolling textures in bcc-metals/alloys consist of a γ-fiber and a part of α-fiber from E to Rotated-cube textures in the ODF section at $\phi_2$ = 45° with a strong maximum for {223}<110> [129–131]. The latter was associated with the principal operative slip system of {011}<111>-type in bcc-crystals [129]. It is interesting to note that the deformation textures evolved in strain-induced martensite, which appears during cold rolling of meta-stable austenite, are similar to the rolling textures of bcc-materials [127]. The orientation of martensite transformed from austenite of brass, Goss and S orientations in accordance to Kurdjumov–Sachs or Nishiyama–Wasserman orientation relationships was shown locating close to the γ-fiber [127]. Thus, the heritable orientations in deformation martensite do not alter substantially from typical textures of rolled ferrite.

The fiber textures in metals/alloys subjected to uniaxial deformation, such as swaging, drawing, extrusion, upsetting, etc., are mainly governed by the principal deformation scheme, e.g., uniaxial tension or compression. The uniaxial deformation textures developed in fcc- or bcc-materials during tension or compression are the reverse to each other because of specific symmetry of slip systems [5,69]. Namely, the fiber textures of <110> or <111> and <100> along the tension or compression axis, respectively, are readily develop in bcc-metals/alloys, whereas <100> and <111> along the tension axis or <110> along the compression axis conversely develop in fcc-materials.

The strong prevalence of basal slip in hcp-metals/alloys results in a sharp <0001> fiber along the compression axis or <0001> crosswise to the tension during uniaxial deformation [132–134]. The features of rolling textures in hp-materials depend significantly on the unit cell parameters, i.e., c/a ratio, which dictates the accommodating non-basal slip and/or twinning. A sharp {0002}<1010> basal texture experiences ±30° split toward transverse direction because of concurrent operation of twinning, prism slip, and pyramidal slip in a cold rolled α-Ti (Figure 22a) [133]. An enhancement of pyramidal <c+a> slip at large rolling reductions further promoted the orientation spread around typical split-basal rolling texture (Figure 22b) [133].

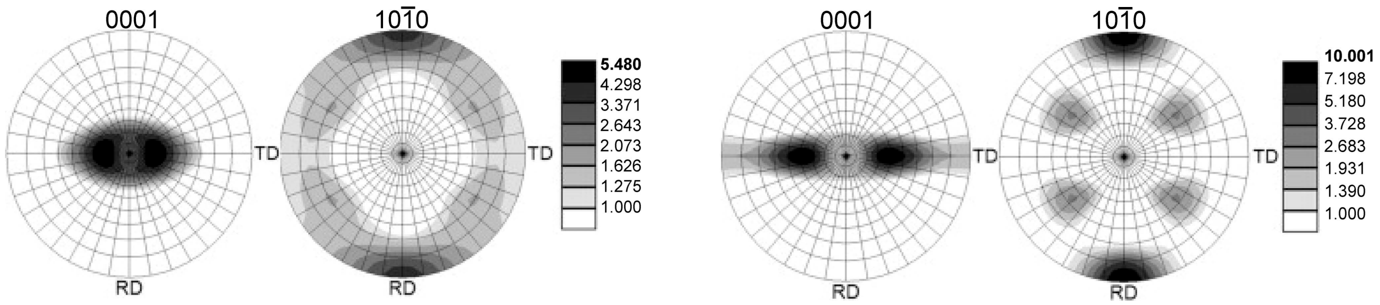


(**a**) (**b**)

**Figure 22.** Pole figures for α-Ti after cold rolling reductions of 75% (**a**) and 95% (**b**) [133].

*4.2. Severe Plastic Deformation*

The frequently used techniques of severe plastic deformation, such as ECAP and HPT, involve a simple shear deformation mode, which is commonly considered as a special feature of such processing [14–16,23]. Li et al. analyzed the ECAP textures in cubic materials by a comparison with simple shear [135]. The main ideal orientations and fiber textures associated with simple shear along the x′ direction (y′-shear plane) are shown in Figure 23 and listed in Tables 3 and 4 for cubic metals/alloys [135]. Note here that {hkl} <uvw> orientations indicated in Tables 3 and 4 denote the {hkl} plane normal to the pressing direction and the <uvw> direction along the outgoing channel of ECAP. Some mismatch between the experimental ECAP textures and the ideal ones was attributed to the deviation of plastic flow from simple shear due to rounded outer corner [136].

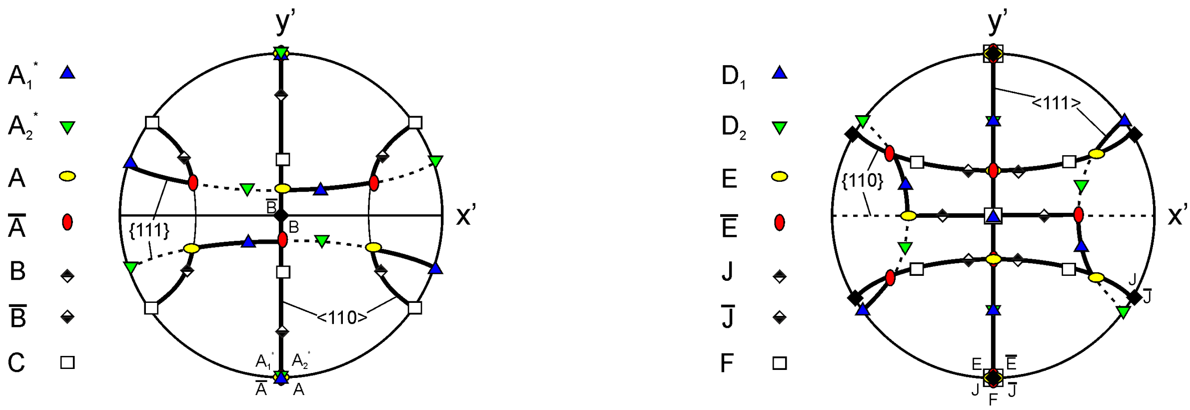


(**a**) (**b**)

**Figure 23.** Main ideal orientations in {111} and {110} pole figures for simple shear deformation of fcc (**a**) and bcc (**b**) metals, respectively [135].

**Table 3.** Main ideal orientations in simple shear deformation of fcc-metals [135].

| Notation | {hkl} <uvw> | Euler Angles | | |
|---|---|---|---|---|
| | | $\varphi_1$ | $\Phi$ | $\varphi_2$ |
| $A_1$* | $(1\,1\,1)\,[\bar{1}\,\bar{1}\,2]$ | 35.26/215.26 | 45 | 0/90 |
| | | 125.26 | 90 | 45 |
| $A_2$* | $(1\,1\,1)\,[1\,1\,\bar{2}]$ | 144.74 | 45 | 0/90 |
| | | 54.74/234.74 | 90 | 45 |
| $A$ | $(1\,\bar{1}\,1)\,[1\,1\,0]$ | 0 | 35.26 | 45 |
| $\bar{A}$ | $(\bar{1}\,1\,\bar{1})\,[\bar{1}\,\bar{1}\,0]$ | 180 | 35.26 | 45 |
| $B$ | $(1\,\bar{1}\,2)\,[1\,1\,0]$ | 0/120/240 | 54.74 | 45 |
| $\bar{B}$ | $(\bar{1}\,1\,\bar{2})\,[\bar{1}\,\bar{1}\,0]$ | 60/180 | 54.74 | 45 |
| $C$ | {0 0 1} <1 1 0> | 90/270 | 45 | 0/90 |
| | | 0/180 | 90 | 45 |

**Table 4.** Main ideal orientations in simple shear deformation of bcc-metals [135].

| Notation | {hkl} <uvw> | Euler Angles | | |
|---|---|---|---|---|
| | | $\varphi_1$ | $\Phi$ | $\varphi_2$ |
| $D_1$ | $(\bar{1}\,\bar{1}\,2)\,[1\,1\,1]$ | 54.74/2334.74 | 45 | 0/90 |
| | | 144.74 | 90 | 45 |
| $D_2$ | $(1\,1\,\bar{2})\,[1\,1\,1]$ | 125.26 | 45 | 0/90 |
| | | 35.26/215.26 | 90 | 45 |
| $E$ | $(1\,1\,0)\,[1\,\bar{1}\,1]$ | 90 | 35.26 | 45 |
| $\bar{E}$ | $(\bar{1}\,\bar{1}\,0)\,[\bar{1}\,1\,\bar{1}]$ | 270 | 35.26 | 45 |
| $J$ | $(1\,1\,0)\,[1\,\bar{1}\,2]$ | 90/120 | 54.74 | 45 |
| $\bar{J}$ | $(\bar{1}\,\bar{1}\,0)\,[\bar{1}\,1\,\bar{2}]$ | 30/150/270 | 54.74 | 45 |
| $F$ | {1 1 0} <0 0 1> | 0/180 | 45 | 0/90 |
| | | 90/270 | 90 | 45 |

The change in the strain path in ECAP experiments resulted in the deformation textures of moderate intensity even after large total strains (Figure 24) [137]. The strong {hkl}<110> fiber developed in an aluminum alloy at relatively low temperatures was alternated with {112}<110> textures with an increase in ECAP temperature [137]. The change in the ECAP route does not significantly affect the development of ECAP texture in bcc-metals/alloys (Figure 25) [138]. The development of {110}<uvw> and {hkl}<111> fibers was observed irrespective of the ECAP routes. Quantitatively, the orientation distribution along these fibers was more uniform when the ECAP sample was pressed without rotation or rotated through 180° between pressings than in the ECAP samples rotated by 90° [138].

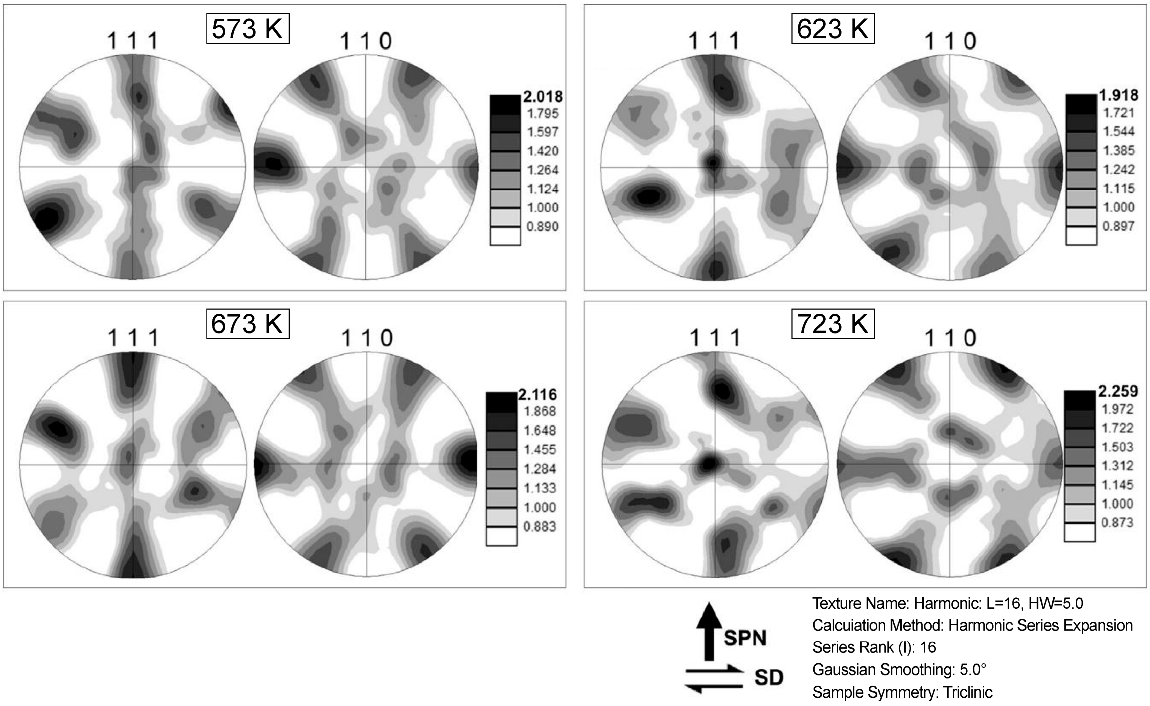


**Figure 24.** Pole figures for an Al-Mg-Sc alloy subjected to 12 ECAP passes at different temperatures [137].

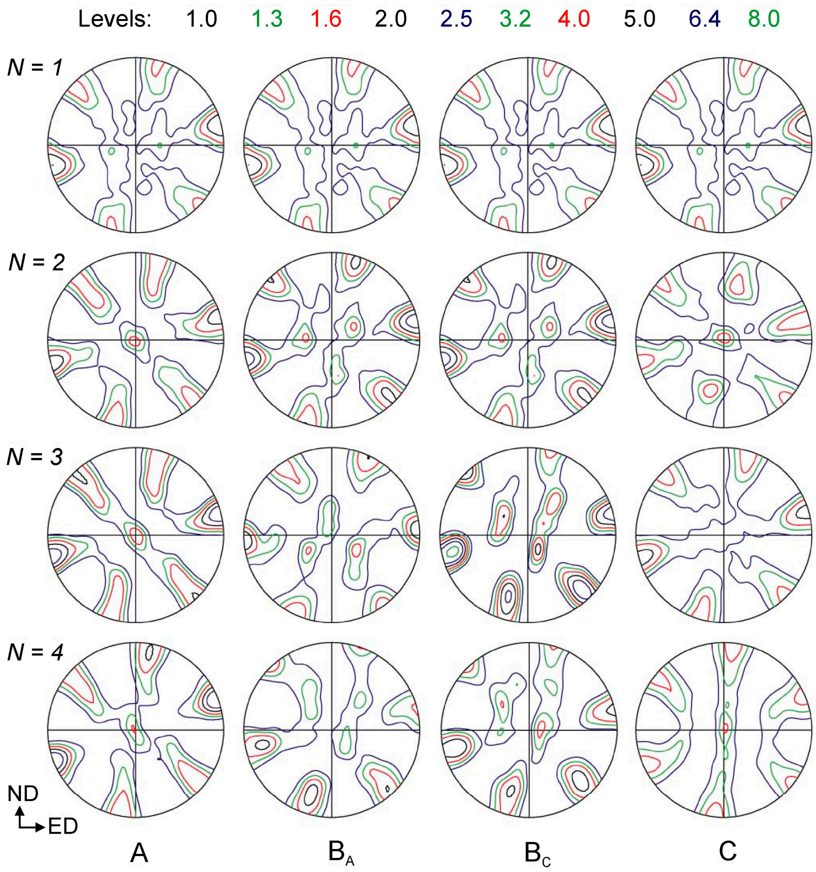


**Figure 25.** {110} Pole figures for an IF-steel subjected to $N$ = 1 to 4 ECAP passes via routes of A, $B_A$, $B_C$, or C [138].

Except for HPT based on simple shear deformation, other techniques of severe plastic deformation do not lead to the development of strong specific texture. The complicated strain states in various sophisticated deformation techniques result from a varying diversity of the deformation mechanisms; each of them reorients respective crystallites toward definite stable orientations. Therefore, the developing deformation texture involves a number of different components with nearly the same intensity. For instance, the deformation textures evolved in an Al-Mg-Sc alloy subjected to friction stir processing are illustrated in Figure 26 [137]. Note here that the pole figures were rotated to align their reference frames with presumed simple shear geometry. It is clearly seen in Figure 26 that the crystallites orientations did not exhibit any remarkable components caused by severe deformation irrespective of processing regimes.

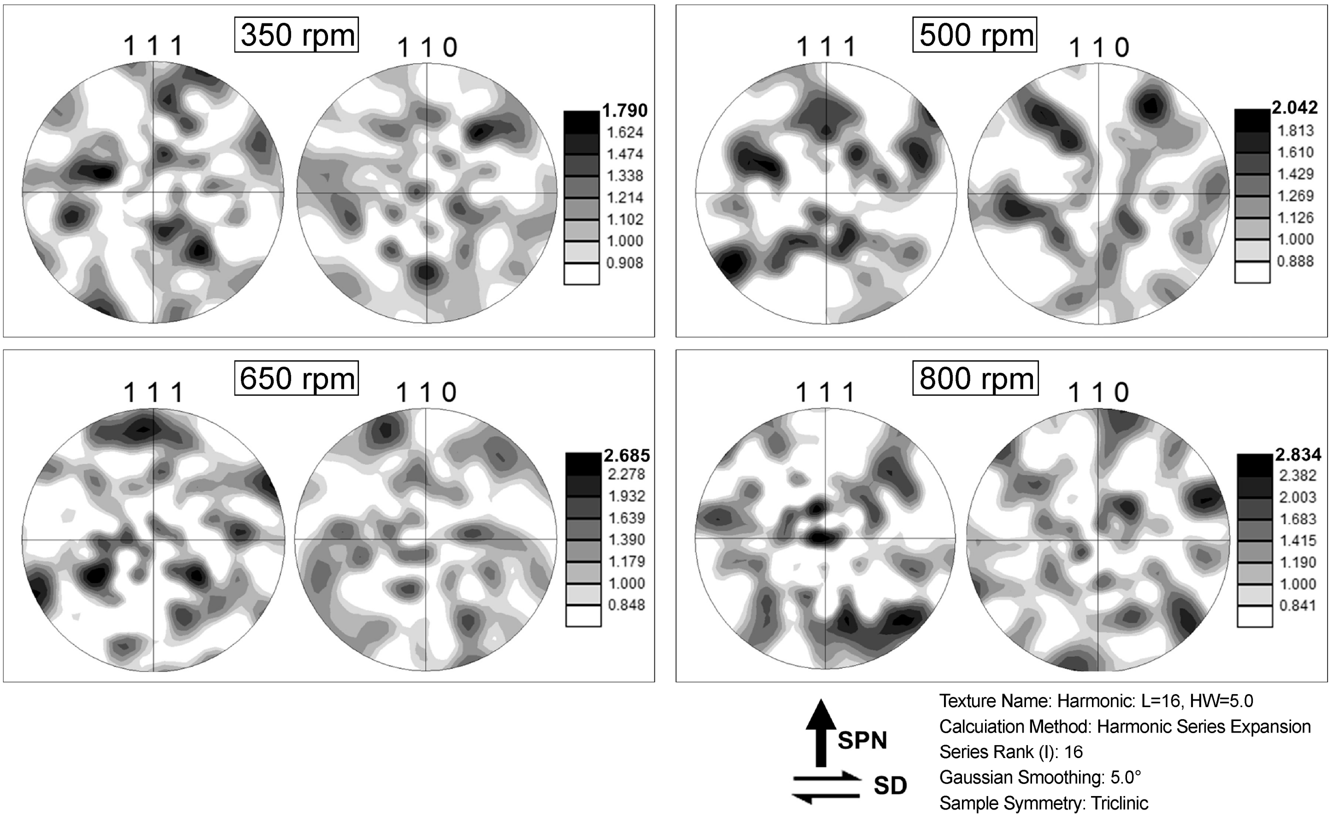


**Figure 26.** Pole figures for an Al-Mg-Sc alloy subjected to friction stir processing at different tool-rotation speeds [137].

## 5. Mechanical Properties

Generally, cold-to-warm working results in significant strengthening that is accompanied by a degradation of plasticity [55,127–129,139–141]. The tensile stress–strain curves for the work hardened steels and alloys are commonly characterized by a sharp strengthening stage at deformation beginning, when the flow stress increases to its maximum at relatively small strain, followed by gradual decrease in the stress caused by necking and failure (Figure 27) [55,139]. An increase in the strain during cold-to-warm working increases both the yield strength and ultimate tensile strength (UTS) of processed semi-products, although the processing effect on the yield strength is much more pronounced as compared to that on UTS (Figure 27a). Thus, the yield strength of cold/warm worked steels/alloys tends to approach UTS, shortening the uniform elongation associated with the stage of initial strengthening with increasing the strain of cold/warm deformation. The strengthening efficiency of cold-to-warm working decreases with an increase in deformation temperature (Figure 27b). An increase in deformation temperature to hot-working conditions is accompanied by a decrease in the work hardening down to its almost complete disappearance; however, a kind of retained work hardening was reported for DRX microstructures after hot deformation [142,143].

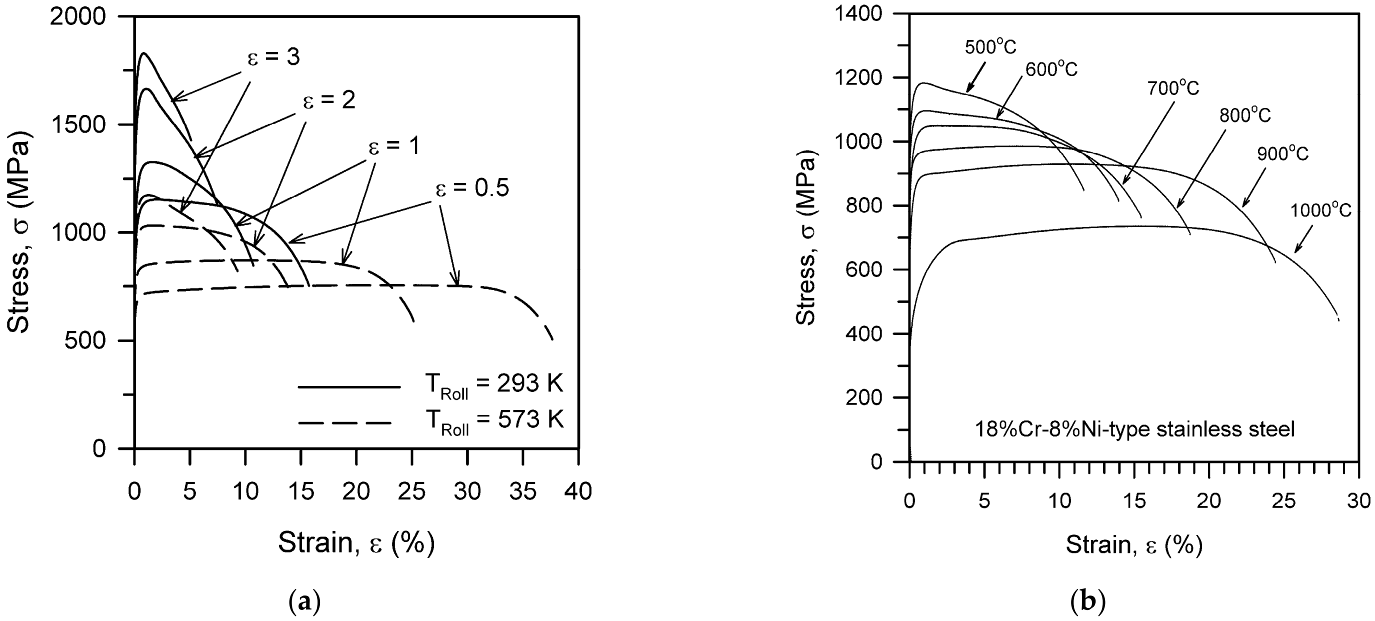


**Figure 27.** Tensile stress–strain curves for a 316L-type stainless steel subjected to rolling to indicated strains (**a**) [55] and an S304H-type stainless steel subjected to rolling to strains of 2.0 at indicated temperatures (**b**) [139].

Structural steel and alloys processed by large-strain cold-to-warm working are characterized by high density of dislocations and grain/subgrain boundaries. The latter ones can be associated with grain refinement or microbanding that involves lattice reorientations. Hence, two main mechanisms are referred to while discussing the strengthening by large strain deformation [55,74,128,139,142–144]. Those are the grain size (or grain boundary or structural) strengthening and the dislocation (or substructural) strengthening. The grain size strengthening ($\sigma_G$) can be expressed by the second term of the well-known Hall–Petch relationship [145,146].

$$\sigma_G = k_y D^{-0.5} \tag{8}$$

where D is the mean grain size, and $k_y$ is the grain boundary strengthening factor. The latter varies over a wide range, from about 70 to 1800 MPa $\mu m^{0.5}$ for different materials [147]. In austenite, $k_y$ reportedly comprises 240–395 Mpa $\mu m^{0.5}$ [148], whereas it depends significantly on the carbon content (C, ppm) in ferrite, i.e., $k_y = 100 + 120\, C^{0.31}$, that gives $k_y$ of 100 to 600 Mpa $\mu m^{0.5}$ [149].

The dislocation strengthening ($\sigma_\rho$), which is also known as work-hardening, should obey Taylor-type relationships [150,151]:

$$\sigma_\rho = \alpha_1 G b \rho^{0.5} \text{ and/or } \sigma_\rho = \alpha_2 G d^{-1} \tag{9}$$

where $\alpha_1$ and $\alpha_2$ are numerical factors, G is the shear modulus, b is the Burgers vector, ρ is the dislocation density, and d is the subgrain size. Moreover, an $\alpha_1$ of about 0.7 was frequently used for various materials [74,88,144]; it can be represented as a product of the dislocation strengthening factor (α of about 0.24) and Taylor factor (M = 2.75 for bcc-metals or M = 3.06 for fcc-metals), i.e., $\alpha_1 = \alpha M$. The work-hardening has been fairly well predicted via either dislocation density or subgrain size in some experimental studies, using accurate methods for the measurement of substructural parameters [150,152–155].

The dislocation density and the subgrain size have also been used together to evaluate the work-hardening [96].

The strengthening mechanisms mentioned above are usually considered as independent and linearly additive [96,154,155]. Such an approach gives good correspondence with experiments involving annealed and recrystallized metals/alloys [142–144,156]. However, summation of the grain size and dislocation strengthening results in well-overestimated strength for cold/warm worked metallic materials [154]. The strengthening of work-hardened materials can be predicted by the combination of the grain size and dislocation strengthening, provided that the strengthening factors (one or both) are reduced to fit the experimental data [55,139]. Moreover, the experimental evaluation of the strengthening factors is hampered by a linear relationship between the grain boundary strengthening and the dislocation strengthening in cold/warm-worked metallic materials [96,98]. Recently, Takaki et al. concluded that the strengthening of work-hardened steels is solely governed by the dislocation density, which incorporates the grain size strengthening and, therefore, can be used to evaluate the strengthening, ignoring the grain-size contribution [157]. Considering the relationship between the grain size and the dislocation density in severely strained metals, Starink also suggested that the strengthening can be predicted through the dislocation density or the grain size [158].

Besides the strengthening, warm working to large strains increases the impact toughness [159]. The thermomechanical treatment consisting of large strain rolling of meta-stable austenite prior bainite/martensite transformation has been called ausforming [160]. Superior mechanical properties of steels subjected to ausforming, followed by quenching and tempering, was attributed to the dislocation substructure transferred from austenite to martensite [161]. Kimura et al. applied large-strain warm rolling, following tempering of carbon steels [162,163]. Such a processing method, which was referred to as tempforming, resulted in the formation of a submicrocrystalline lamella-type microstructure with a uniform dispersion of secondary-phase particles, providing an outstanding combination of mechanical properties [159]. The dispersed particles and the grain refinement, along with the corresponding increase in the dislocation density during warm working, result in significant strengthening [164]. The strengthening by tempforming is accompanied by an increase in the impact toughness, especially at low temperatures, when the impact toughness surprisingly increases with a decrease in the test temperature, owing to delamination of layered microstructure [163]. It should be noted that, besides the expected increase in the strength, the impact toughness also increases with a decrease in the tempforming temperature and/or an increase in the total strain during tempforming [165,166]. The improving effect that the tempforming strain had on the impact toughness was attributed to the change in the coherent cleavage plane length along and across the specimen, leading to a decrease in the cleavage fracture stress in the transverse direction, while that in the rolling direction increased [166].

Finally, one more beneficial property of steels and alloys with fine-grained microstructures developed by large-strain cold-to-warm deformation should be mentioned. Such materials commonly possess improved workability under hot deformation. The most impressive manifestation of this property is superplasticity [167]. Practical application of superplasticity is hindered by a very low strain rate and high temperature that are required for superplastic conditions. The advantage of grain refinement by large-strain cold/warm deformation lies in the fact that the optimal conditions for superplasticity can be extended to a lower temperature [168] and/or a higher strain rate [169], making it quite useful for industrial applications.

## 6. Summary

The large strain deformations under conditions of cold-to-warm working are widely used techniques to enhance the mechanical performance of structural steels and alloys. The close relationship between the deformation regimes and the parameters of developing deformation microstructures open up wide opportunities to control the product properties.

The desired microstructures with beneficial grain and subgrain size, texture, and dislocation density can be obtained in various metallic materials by means of plastic working at appropriate deformation conditions, including processing temperature and strain rate. In turn, the developed microstructures provide a suitable combination of strengthening mechanisms resulting in favorable mechanical properties.

The effect of deformation conditions on the evolved microstructures in various pseudo-single phase steels and alloys has been fairly clarified for the grain/subgrain size, dislocation density, grain boundary misorientations, and textures. Corresponding quantitative approximation of the kinetics of the microstructural changes was being developed along with the expressions for parameters of the deformation microstructures. Recently, successful efforts have been attempted to obtain physically justified interrelations between the microstructural parameters and their dependencies on the strain and processing conditions. Currently, numerous studies are focused on the effect of phase content, especially dispersed precipitations on the deformation microstructures. The main difficulties in the development of the constitutive relationships in dispersion-strengthened steels and alloys are associated with precise evaluation of the particle distribution, including their morphology and the mechanisms of the particle interaction with dislocations and grain/subgrain boundaries. The accurate estimation of the dislocation density in metallic materials subjected to cold/warm deformation is itself a nontrivial task, which requires the selection of adequate approach and usage of appropriate techniques. Moreover, the correct superposition of different strengthening mechanisms is still debatable. Further experimental studies might be quite helpful to solve this problem.

The progress in the field depends on the development of physically justified models of the microstructure—property relationships for complicated metallic systems, such as multiphase dispersion strengthened or composite steels and alloys. The mutual effects of different mechanisms of microstructure evolution on its kinetics in heterogeneous materials deserve further investigation in order to obtain meaningful quantitative expressions for microstructural parameters in advanced materials subjected to cold/warm working. Comprehensive analysis of the microstructural strengthening mechanisms should deal also with their effects on plasticity, because the strength–plasticity combination determines the performance of structural materials in the end. The detailed elaboration of deformation mechanisms, their interaction, and their influence on the deformation behavior seems to be the most important aspect of the current and future investigations in the field.

**Author Contributions:** Conceptualization, M.T. and A.B.; methodology, A.B.; resources, A.D.; writing—original draft preparation, A.B. and A.D.; writing—review and editing, M.T. and A.B.; visualization, A.D.; supervision, R.K.; project administration, R.K. All authors have read and agreed to the published version of the manuscript.

**Funding:** This research was funded by the Russian Science Foundation, Agreement No. 20-19-00497.

**Institutional Review Board Statement:** Not applicable.

**Informed Consent Statement:** Not applicable.

**Data Availability Statement:** The data presented in this study are available upon request from the corresponding author.

**Conflicts of Interest:** The authors declare no conflict of interest.

## References

1. Dieter, G.E. *Mechanical Metallurgy*; McGraw-Hill Book Company: New York, NY, USA, 1961; p. 615.
2. Bernshtein, M.L. *Thermomechanical Treatment of Metals and Alloys*; Metallurgiya: Moscow, Russia, 1968; p. 1172.
3. Zhao, J.; Jiang, Z. Thermomechanical processing of advanced high strength steels. *Prog. Mater. Sci.* **2018**, *94*, 174–242. [CrossRef]
4. Leslie, C.; Hornbogen, E. Physical metallurgy of steels. In *Physical Metallurgy*; Cahn, R.W., Haasen, P., Eds.; Elsevier: Amsterdam, The Netherlands, 1996; pp. 1555–1620.
5. Gil Sevilano, J.; van Houtte, P.; Aernoudt, A. Large strain work hardening and textures. *Prog. Mater. Sci.* **1981**, *25*, 69–412. [CrossRef]

6. Zehetbauer, M. Cold work hardening in stages IV and V of F.C.C. metals—II. Model fits and physical results. *Acta Metall. Mater.* **1993**, *41*, 589–599. [CrossRef]
7. Estrin, Y.; Vinogradov, A. Extreme grain refinement by severe plastic deformation: A wealth of challenging science. *Acta Mater.* **2013**, *61*, 782–817. [CrossRef]
8. Vinogradov, A.; Yasnikov, I.S.; Matsuyama, H.; Uchida, M.; Kaneko, Y.; Estrin, Y. Controlling strength and ductility: Dislocation-based model of necking instability and its verification for ultrafine grain 316L steel. *Acta Mater.* **2016**, *106*, 295–303. [CrossRef]
9. McQueen, H.J.; Jonas, J.J. Recovery and recrystallization during high temperature deformation. In *Treatise on Materials Science and Technology*; Arsenoult, R.J., Ed.; Academic Press: Cambridge, MA, USA, 1975; Volume 6, pp. 393–493. [CrossRef]
10. Maki, T.; Akasaka, T.; Ohkuno, K.; Tamura, I. Dynamic recrystallization of austenite in 18-8 stainless steels and 18Ni maraging steel. *Trans. Iron Steel Jpn.* **1982**, *22*, 253–261. [CrossRef]
11. Sakai, T.; Jonas, J.J. Dynamic recrystallization—Mechanical and microstructural considerations. *Acta Metall.* **1984**, *32*, 189–209. [CrossRef]
12. Humphreys, F.J.; Hatherly, M. *Recrystallization and Related Annealing Phenomena*; Pergamon Press: Oxford, UK, 1996; p. 363.
13. Belyakov, A.; Miura, H.; Sakai, T. Dynamic recrystallization under warm deformation of a 304 type austenitic stainless steel. *Mater. Sci. Eng. A* **1998**, *A255*, 139–147. [CrossRef]
14. Humphreys, F.J.; Prangnell, P.B.; Bowen, J.R.; Gholinia, A.; Harris, C. Developing stable fine-grained microstructures by large strain deformation. *Phil. Trans. R. Soc. Lond.* **1999**, *357*, 1663–1681. [CrossRef]
15. Valiev, R.Z.; Islamgaliev, R.K.; Alexandrov, I.V. Bulk nanostructured materials from severe plastic deformation. *Progr. Mat. Sci.* **2000**, *45*, 103–189. [CrossRef]
16. Segal, V.M.; Reznikov, V.I.; Drobyshevskiy, A.E.; Kopylov, V.I. Plastic metal working by simple shear. *Russ. Metall.* **1981**, *1*, 115–123.
17. Saunders, I.; Nutting, J. Deformation of metals to high strains using combination of torsion and compression. *Met. Sci.* **1984**, *18*, 571–575. [CrossRef]
18. Richert, J.; Richert, M. A new method for unlimited deformation of metals and alloys. *Aluminium* **1986**, *62*, 604–607.
19. Saito, Y.; Tsuji, N.; Utsunomiya, H.; Sakai, T.; Hong, R.G. Ultra-fine grained bulk aluminum produced by accumulative roll-bonding (ARB) process. *Scr. Mater.* **1998**, *39*, 1221–1227. [CrossRef]
20. Takaki, S.; Tsuchiyama, T.; Nakashima, K.; Hidaka, H.; Kawasaki, K.; Futamura, Y. Microstructure development of steel during severe plastic deformation. *Met. Mater. Int.* **2004**, *10*, 533–539. [CrossRef]
21. Langdon, T.G.; Furukawa, M.; Nemoto, M.; Horita, Z. Using equal-channel angular pressing for refining grain size. *JOM* **2000**, *52*, 30–33. [CrossRef]
22. Valiev, R.Z.; Langdon, T.G. Principles of equal-channel angular pressing as a processing tool for grain refinement. *Prog. Mater. Sci.* **2006**, *51*, 881–981. [CrossRef]
23. Zhilyaev, A.P.; Langdon, T.G. Using high-pressure torsion for metal processing: Fundamentals and applications. *Prog. Mater. Sci.* **2008**, *53*, 893–979. [CrossRef]
24. Belyakov, A.; Sakai, T.; Miura, H. Fine-grained structure formation in austenitic stainless steel under multiple deformation at 0.5 Tm. *Mater. Trans. JIM* **2000**, *41*, 476–484. [CrossRef]
25. Belyakov, A.; Sakai, T.; Miura, H.; Tsuzaki, K. Grain refinement in copper under large strain deformation. *Philos. Mag. A* **2001**, *81*, 2629–2643. [CrossRef]
26. Ivanisenko, Y.; Lojkowski, W.; Valiev, R.Z.; Fecht, H.-J. The mechanism of formation of nanostructure and dissolution of cementite in a pearlitic steel during high pressure torsion. *Acta Mater.* **2003**, *51*, 5555–5570. [CrossRef]
27. Xu, C.; Furukawa, M.; Horita, Z.; Langdon, T.G. The evolution of homogeneity and grain refinement during equal-channel angular pressing: A model for grain refinement in ECAP. *Mater. Sci. Eng. A* **2005**, *A398*, 66–76. [CrossRef]
28. Raab, G.J.; Valiev, R.Z.; Lowe, T.C.; Zhu, Y.T. Continuous processing of ultrafine grained Al by ECAP–Conform. *Mater. Sci. Eng. A* **2004**, *A382*, 30–34. [CrossRef]
29. Tsuji, N.; Saito, Y.; Lee, S.-H.; Minamino, Y. ARB (Accumulative Roll-Bonding) and other new techniques to produce bulk ultrafine grained materials. *Adv. Eng. Mater.* **2003**, *5*, 338–344. [CrossRef]
30. Zherebtsov, S.V.; Salishchev, G.A.; Galeyev, R.M. Formation of submicrocrystalline structure in titanium and its alloy under severe plastic deformation. *Defect Diffus. Forum* **2002**, *208–209*, 237–240. [CrossRef]
31. Shrivastava, S.C.; Jonas, J.J.; Canova, G. Equivalent strain in large deformation testing: Theoretical and practical considerations. *J. Mech. Phys. Solids* **1982**, *30*, 75–90. [CrossRef]
32. Kimura, Y.; Takaki, S. Microstructural changes during annealing of work-hardened mechanically milled metallic powders. *Mater. Trans. JIM* **1995**, *36*, 289–296. [CrossRef]
33. Koch, C.C. Synthesis of nanostructured materials by mechanical milling: Problems and opportunities. *Nanostruct. Mater.* **1997**, *9*, 13–22. [CrossRef]
34. Huang, J.Y.; Zhu, Y.T.; Jiang, H.; Lowe, T.C. Microstructures and dislocation configurations in nanostructured Cu processed by repetitive corrugation and straightening. *Acta Mater.* **2001**, *49*, 1497–1505. [CrossRef]
35. Suh, D.W.; Torizuka, S.; Ohmori, A.; Inoue, T.; Nagai, K. Dynamic restoration process of Ni–30Fe alloy during hot deformation. *ISIJ Int.* **2002**, *42*, 432–439. [CrossRef]

36. Takayama, Y.; Miura, T.; Kato, H.; Watanabe, H. Microstructural and textural evolution by continuous cyclic bending and annealing in a high purity titanium. *Mater. Trans.* **2004**, *45*, 2826–2831. [CrossRef]
37. Toth, L.S.; Arzaghi, M.; Fundenberger, J.J.; Beausir, B.; Bouaziz, O.; Arruffat-Massion, R. Severe plastic deformation of metals by high-pressure tube twisting. *Scr. Mater.* **2009**, *60*, 175–177. [CrossRef]
38. Wadsworth, J.; Sherby, O.D. On the bulat—Damascus steels revisited. *Prog. Mater. Sci.* **1980**, *25*, 35–68. [CrossRef]
39. Salishchev, G.A.; Valiakhmetov, O.R.; Galeyev, R.M. Formation of submicrocrystalline structure in the titanium alloy VT8 and its influence on mechanical properties. *J. Mater. Sci.* **1993**, *28*, 2898–2902. [CrossRef]
40. Belyakov, A.; Gao, W.; Miura, H.; Sakai, T. Strain induced grain evolution in polycrystalline copper during warm deformation. *Metall. Mater. Trans. A* **1998**, *29A*, 2957–2965. [CrossRef]
41. Belyakov, A.; Kimura, Y.; Adachi, Y.; Tsuzaki, K. Microstructure evolution in ferritic stainless steels during large strain deformation. *Mater. Trans.* **2004**, *45*, 2812–2821. [CrossRef]
42. Williams, D.B.; Carter, C.B. *Transmission Electron Microscopy*; Plenum Press: New York, NY, USA, 1996; p. 730.
43. Belyakov, A.; Dudova, N.; Tikhonova, M.; Sakai, T.; Tsuzaki, K.; Kaibyshev, R. Dynamic recrystallization mechanisms operating under different processing conditions. *Mater. Sci. Forum* **2012**, *706–709*, 2704–2709. [CrossRef]
44. Humphreys, F.J. Quantitative metallography by electron backscattered diffraction. *J. Microsc.* **1999**, *195*, 170–185. [CrossRef]
45. Schwartz, A.J.; Kumar, M.; Adams, B.L.; Field, D.P. *Electron. Backscatter Diffraction in Materials Science*; Springer: New York, NY, USA, 2009; p. 406.
46. Zisman, A.; Zolotorevsky, N.; Petrov, S.; Hlusova, E.; Yashina, E. Panoramic crys-tallographic analysis of structure evolution in low-carbon martensitic steel under tempering. *Metal Sci. Heat Treat.* **2018**, *60*, 142–149. [CrossRef]
47. Calcagnotto, M.; Ponge, D.; Demir, E.; Raabe, D. Orientation gradients and geometrically necessary dislocations in ultrafine grained dual-phase steels studied by 2D and 3D EBSD. *Mater. Sci. Eng. A* **2010**, *A527*, 2738–2746. [CrossRef]
48. Konijnenberg, P.J.; Zaefferer, S.; Raabe, D. Assessment of geometrically necessary dislocation levels derived by 3D EBSD. *Acta Mater.* **2015**, *99*, 402–414. [CrossRef]
49. Ermakova, N.Y.; Zolotorevsky, N.Y.; Titovets, Y.F. Quantitative X-ray analysis of deformation microtexture within individual grains. *Mater. Sci. Forum* **2005**, *495–497*, 983–988. [CrossRef]
50. Sauvage, X.; Enikeev, N.; Valiev, R.; Nasedkina, Y.; Murashkin, M. Atomic-scale analysis of the segregation and precipitation mechanisms in a severely deformed Al–Mg alloy. *Acta Mater.* **2014**, *72*, 125–136. [CrossRef]
51. Belyakov, A.; Tsuzaki, K.; Kimura, Y.; Kimura, Y.; Mishima, Y. Comparative study on microstructure evolution upon unidirectional and multidirectional cold working in an Fe—15%Cr ferritic alloy. *Mater. Sci. Eng. A* **2007**, *A456*, 323–331. [CrossRef]
52. Tikhonova, M.; Shakhova, I.; Kaibyshev, R.; Belyakov, A. Effect of SPD processing technique on grain refinement and properties of an austenitic stainless steel. *Mater. Sci. Forum* **2017**, *879*, 1957–1962. [CrossRef]
53. Belyakov, A.; Tsuzaki, K.; Kimura, Y. Regularities of deformation microstructures in ferritic stainless steels during large strain cold working. *ISIJ Int.* **2008**, *48*, 1071–1079. [CrossRef]
54. Sakai, T.; Belyakov, A.; Miura, H. Ultrafine grain refinement in ferritic stainless steel during severe plastic deformation. *Metall. Mater. Trans. A* **2008**, *39A*, 2206–2214. [CrossRef]
55. Odnobokova, M.; Belyakov, A.; Kaibyshev, R. Effect of severe cold or warm deformation on microstructure evolution and tensile behavior of a 316L stainless steel. *Adv. Eng. Mater.* **2015**, *17*, 1812–1820. [CrossRef]
56. Belyakov, A.; Murayama, M.; Sakai, Y.; Tsuzaki, K.; Okubo, M.; Eto, M.; Kimura, T. Development of a high-strength high-conductivity Cu-Ni-P alloy, Part II: Processing by severe deformation. *J. Electr. Mater.* **2006**, *35*, 2000–2008. [CrossRef]
57. Sakai, T.; Belyakov, A.; Kaibyshev, R.; Miura, H.; Jonas, J.J. Dynamic and post-dynamic recrystallization under hot, cold and severe plastic deformation conditions. *Prog. Mater. Sci.* **2014**, *60*, 130–207. [CrossRef]
58. Hornbogen, E.; Koster, U. Recrystallization of two-phase alloys. In *Recrystallization of Metallic Materials*; Haessner, F., Ed.; Riederer-Verlag GmbH: Stuttgart, Germany, 1978; pp. 159–194.
59. Gardner, K.J.; Grimes, R. Recrystallization during hot deformation of aluminium alloys. *Met. Sci.* **1979**, *13*, 216–222. [CrossRef]
60. Maki, T.; Okaguchi, S.; Tamura, I. Dynamic recrystallization in ferritic stainless steel. In *Strength of Metals and Alloys (ICSMA 6)*; Gifkins, R.C., Ed.; Pergamon Press: Oxford, UK, 1982; pp. 529–534. [CrossRef]
61. Belyakov, A.; Kaibyshev, R.; Sakai, T. New grain formation during warm deformation of ferritic stainless steel. *Metall. Mater. Trans. A* **1998**, *29A*, 161–167. [CrossRef]
62. Galiev, A.; Kaibyshev, R.; Gottstein, G. Correlation of plastic deformation and dynamic recrystallization in magnesium alloy ZK60. *Acta Mater.* **2001**, *49*, 1199–1207. [CrossRef]
63. Sitdikov, O.; Kaibyshev, R. Dynamic recrystallization in pure magnesium. *Mater. Trans.* **2001**, *42*, 1928–1937. [CrossRef]
64. Rybin, V.V. *Large Plastic Deformations and Destruction of Metals*; Metallurgia: Moscow, Russia, 1987; p. 224. [CrossRef]
65. Tikhonova, M.; Kaibyshev, R.; Fang, X.; Wang, W.; Belyakov, A. Grain boundary assembles developed in an austenitic stainless steel during large strain warm working. *Mater. Character* **2012**, *70*, 14–20. [CrossRef]
66. Tikhonova, M.; Belyakov, A.; Kaibyshev, R. Strain-induced grain evolution in an austenitic stainless steel under warm multiple forging. *Mater. Sci. Eng. A* **2013**, *A564*, 413–422. [CrossRef]
67. Shakhova, I.; Yanushkevich, Z.; Fedorova, I.; Belyakov, A.; Kaibyshev, R. Grain refinement in a Cu-Cr-Zr alloy during multidirectional forging. *Mater. Sci. Eng. A* **2014**, *A606*, 380–389. [CrossRef]

68. Kuhlmann-Wilsdorf, D.; Hansen, N. Geometrically necessary, incidental and subgrain boundaries. *Scr. Metall. Mater.* **1991**, *25*, 1557–1562. [CrossRef]
69. Belyakov, A.; Kimura, Y.; Tsuzaki, K. Microstructure evolution in dual phase stainless steel during severe deformation. *Acta Mater.* **2006**, *54*, 2521–2532. [CrossRef]
70. Yu, T.; Hansen, N.; Huang, X. Linking recovery and recrystallization through triple junction motion in aluminum cold rolled to a large strain. *Acta Mater.* **2013**, *61*, 6577–6586. [CrossRef]
71. Renk, O.; Hohenwarter, A.; Wurster, S.; Pippan, R. Direct evidence for grain boundary motion as the dominant restoration mechanism in the steady-state regime of extremely cold-rolled copper. *Acta Mater.* **2014**, *77*, 401–410. [CrossRef] [PubMed]
72. Toth, L.S.; Estrin, Y.; Lapovok, R.; Gu, C. A model of grain fragmentation based on lattice curvature. *Acta Mater.* **2010**, *58*, 1782–1794. [CrossRef]
73. Belyakov, A.; Tsuzaki, K.; Miura, H.; Sakai, T. Effect of initial microstructures on grain refinement in a stainless steel by large strain deformation. *Acta Mater.* **2003**, *51*, 847–861. [CrossRef]
74. Morozova, A.; Kaibyshev, R. Grain refinement and strengthening of a Cu–0.1Cr–0.06Zr alloy subjected to equal channel angular pressing. *Philos. Mag.* **2017**, *97*, 2053–2076. [CrossRef]
75. Odnobokova, M.; Belyakov, A.; Enikeev, N.; Kaibyshev, R.; Valiev, R.Z. Microstructural changes and strengthening of austenitic stainless steels during rolling at 473 K. *Metals* **2020**, *10*, 1614. [CrossRef]
76. Beladi, H.; Cizek, P.; Hodgson, P.D. Dynamic recrystallization of austenite in Ni-30 Pct Fe model alloy: Microstructure and texture evolution. *Metall. Mater. Trans. A* **2009**, *40A*, 1175–1189. [CrossRef]
77. Dudova, N.; Belyakov, A.; Sakai, T.; Kaibyshev, R. Dynamic recrystallization mechanisms operating in a Ni–20%Cr alloy under hot-to-warm working. *Acta Mater.* **2010**, *58*, 3624–3632. [CrossRef]
78. Belyakov, A.; Zherebtsov, S.; Salishchev, G. Three-stage relationship between flow stress and dynamic grain size in titanium in a wide temperature interval. *Mater. Sci. Eng. A* **2015**, *A628*, 104–109. [CrossRef]
79. Tikhonova, M.; Enikeev, N.; Valiev, R.Z.; Belyakov, A.; Kaibyshev, R. Submicrocrystalline Austenitic Stainless Steel Processed by Cold or Warm High Pressure Torsion. *Mater. Sci. Forum* **2016**, *838–839*, 398–403. [CrossRef]
80. Gholizadeh, R.; Shibata, A.; Tsuji, N. Global view for grain refinement in ultra-low-C IF steel during high-strain deformation at various temperatures and strain rates. *Materialia* **2019**, *6*, 100262. [CrossRef]
81. Young, C.M.; Sherby, O.D. Subgrain formation and subgrain-boundary strengthening in iron-based materials. *J. Iron Steel Inst.* **1973**, *211*, 640–647.
82. Taylor, G.I. The mechanism of plastic deformation of crystals. Part I.—Theoretical. *Proc. R. Soc. Lond. A* **1934**, *145*, 362–387. [CrossRef]
83. Hansen, N. Polycrystalline strengthening. *Metall. Trans. A* **1985**, *16A*, 2167–2190. [CrossRef]
84. Hansen, N.; Huang, X. Microstructure and flow stress of polycrystals and single crystals. *Acta Mater.* **1998**, *46*, 1827–1836. [CrossRef]
85. Mecking, H.; Kocks, U.F. Kinetics of flow and strain-hardening. *Acta Metall.* **1981**, *29*, 1865–1875. [CrossRef]
86. Estrin, Y.; Mecking, H. A unified phenomenological description of work hardening and creep based on one-parameter models. *Acta Metall.* **1984**, *32*, 57–70. [CrossRef]
87. Jonas, J.J.; Quelennec, X.; Jiang, L.; Martin, E. The Avrami kinetics of dynamic recrystallization. *Acta Mater.* **2009**, *57*, 2748–2756. [CrossRef]
88. Zhilyaev, A.P.; Shakhova, I.; Morozova, A.; Belyakov, A.; Kaibyshev, R. Grain refinement kinetics and strengthening mechanisms in Cu–0.3Cr–0.5Zr alloy subjected to intense plastic deformation. *Mater. Sci. Eng. A* **2016**, *A654*, 131–142. [CrossRef]
89. Valiev, R.Z.; Korznikov, A.V.; Mulyukov, R.R. Structure and properties of ultrafine-grained materials produced by severe plastic deformation. *Mater. Sci. Eng. A* **1993**, *A168*, 141–148. [CrossRef]
90. Belyakov, A.; Sakai, T.; Miura, H.; Kaibyshev, R. Substructures and internal stresses developed under warm severe deformation of austenitic stainless steel. *Scripta Mater.* **2000**, *42*, 319–325. [CrossRef]
91. Belyakov, A.; Sakai, T.; Miura, H.; Kaibyshev, R. Strain-induced submicrocrystalline grains developed in austenitic stainless steel under severe warm deformation. *Philos. Mag. Lett.* **2000**, *80*, 711–718. [CrossRef]
92. Romanov, A.E.; Vladimirov, V.I. Disclinations in crystalline solids. In *Dislocation in Solids*; Nabarro, F.R.N., Ed.; Elsevier Science: Amsterdam, The Netherlands, 1992; Volume 9, pp. 191–402.
93. Rybin, V.V.; Zisman, A.A.; Zolotorevsky, N.Y. Junction disclinations in plastically deformed crystals. *Acta Mater.* **1993**, *41*, 2211–2217. [CrossRef]
94. Zisman, A. Model for partitioning slip patterns at triple junctions of grains. *Int. J. Eng. Sci.* **2017**, *116*, 155–164. [CrossRef]
95. Belyakov, A.; Sakai, T.; Miura, H.; Kaibyshev, R. Grain refinement under multiple warm deformation in 304 type austenitic stainless steel. *ISIJ Int.* **1999**, *39*, 592–599. [CrossRef]
96. Yanushkevich, Z.; Dobatkin, S.V.; Belyakov, A.; Kaibyshev, R. Hall-Petch relationship for austenitic stainless steels processed by large strain warm rolling. *Acta Mater.* **2017**, *136*, 39–48. [CrossRef]
97. Morozova, A.; Mishnev, R.; Belyakov, A.; Kaibyshev, R. Microstructure and properties of fine grained Cu-Cr-Zr alloys after thermo-mechanical treatments. *Rev. Adv. Mater. Sci.* **2018**, *54*, 56–92. [CrossRef]

98. Tikhonova, M.; Torganchuk, V.; Brasche, F.; Molodov, D.A.; Belyakov, A.; Kaibyshev, R. Effect of warm to hot rolling on microstructure, texture and mechanical properties of an advanced medium-Mn steel. *Metall. Mater. Trans. A* **2019**, *50A*, 4245–4256. [CrossRef]
99. Dolzhenko, P.; Tikhonova, M.; Kaibyshev, R.; Belyakov, A. Peculiarities of DRX in a highly-alloyed austenitic stainless steel. *Materials* **2021**, *14*, 4004. [CrossRef]
100. Tsuji, N.; Ueji, R.; Minamino, Y.; Saito, Y. A new and simple process to obtain nano-structured bulk low-carbon steel with superior mechanical property. *Scr. Mater.* **2002**, *46*, 305–310. [CrossRef]
101. Korshunov, A.A.; Enikeev, F.U.; Mazurski, M.I.; Salishchev, G.A.; Dmitriev, O.V.; Muravlev, A.V.; Chistyakov, P.V. Grain-structure refinement in titanium alloy under different loading schedules. *J. Mater. Sci.* **1996**, *31*, 4635–4639. [CrossRef]
102. Goloborodko, A.; Sitdikov, O.; Kaibyshev, R.; Miura, H.; Sakai, T. Effect of pressing temperature on fine-grained structure formation in 7475 aluminum alloy during ECAP. *Mater. Sci. Eng. A* **2004**, *A381*, 121–128. [CrossRef]
103. Narayana Murty, S.V.S.; Torizuka, S.; Nagai, K. Ferrite grain size formed by large strain-high Z deformation in a 0.15C steel. *Mater. Trans.* **2005**, *46*, 2454–2460. [CrossRef]
104. Iwahashi, Y.; Horita, Z.; Nemoto, M.; Langdon, T.G. An investigation of microstructural evolution during equal-channel angular pressing. *Acta Mater.* **1997**, *45*, 4733–4741. [CrossRef]
105. Iwahashi, Y.; Horita, Z.; Nemoto, M.; Langdon, T.G. The process of grain refinement in equal-channel angular pressing. *Acta Mater.* **1998**, *46*, 3317–3331. [CrossRef]
106. Tikhonova, M.; Dolzhenko, P.; Kaibyshev, R.; Belyakov, A. Grain boundary assemblies in dynamically-recrystallized austenitic stainless steel. *Metals* **2016**, *6*, 268. [CrossRef]
107. Jafari, M.; Najafizadeh, A. Correlation between Zener-Hollomon parameter and necklace DRX during hot deformation of 316 stainless steel. *Mater. Sci. Eng. A* **2009**, *A501*, 16–25. [CrossRef]
108. Beladi, H.; Cizek, P.; Hodgson, P.D. On the characteristics of substructure development through dynamic recrystallization. *Acta Mater.* **2010**, *58*, 3531–3541. [CrossRef]
109. Belyakov, A.; Tikhonova, M.; Yanushkevich, Z.; Kaibyshev, R. Regularities of grain refinement in an austenitic stainless steel during multiple warm working. *Mater. Sci. Forum* **2013**, *753*, 411–416. [CrossRef]
110. Yanushkevich, Z.; Lugovskaya, A.; Belyakov, A.; Kaibyshev, R. Deformation microstructures and tensile properties of an austenitic stainless steel subjected to multiple warm rolling. *Mater. Sci. Eng. A* **2016**, *A667*, 279–285. [CrossRef]
111. Dolzhenko, A.; Pydrin, A.; Gaidar, S.; Kaibyshev, R.; Belyakov, A. Microstructure and strengthening mechanisms in an hsla steel subjected to tempforming. *Metals* **2022**, *12*, 48. [CrossRef]
112. Ryan, N.D.; McQueen, H.J.; Jonas, J.J. The deformation behavior of types 304, 316, and 317 austenitic stainless steels during hot torsion. *Can. Metall. Q.* **1983**, *22*, 369–378. [CrossRef]
113. Ryan, N.D.; McQueen, H.J. Dynamic softening mechanisms in 304 austenitic stainless steel. *Can. Metall. Q.* **1990**, *29*, 147–162. [CrossRef]
114. Tikhonova, M.; Kaibyshev, R.; Belyakov, A. Microstructure and mechanical properties of austenitic stainless steels after dynamic and post-dynamic recrystallization treatment. *Adv. Eng. Mater.* **2018**, *20*, 1700960. [CrossRef]
115. Bay, B.; Hansen, N.; Hughes, D.A.; Kuhlmann-Wilsdorf, D. Evolution of f.c.c. deformation structures in polyslip. *Acta Metall. Mater.* **1992**, *40*, 205–219. [CrossRef]
116. Kobayashi, C.; Sakai, T.; Belyakov, A.; Miura, H. Ultrafine grain development in copper during multi-directional forging at 195 K. *Philos. Mag. Lett.* **2007**, *87*, 751–766. [CrossRef]
117. Tsuzaki, K.; Xiaoxu, H.; Maki, T. Mechanism of dynamic continuous recrystallization during superplastic deformation in a microduplex stainless steel. *Acta Mater.* **1996**, *44*, 4491–4499. [CrossRef]
118. Qing, L.; Xiaoxu, H.; Mei, Y.; Jinfeng, Y. On deformation-induced continuous recrystallization in a superplastic AlLiCuMgZr alloy. *Acta Metall. Mater.* **1992**, *40*, 1753–1762. [CrossRef]
119. Yanushkevich, Z.; Belyakov, A.; Kaibyshev, R. Microstructural evolution of a 304-type austenitic stainless steel during rolling at temperatures of 773–1273 K. *Acta Mater.* **2015**, *82*, 244–254. [CrossRef]
120. Sakai, T.; Miura, H. Ultrafine grain formation in aluminum alloys during hot severe plastic deformation. *Mater. Sci. Forum* **2012**, *706–709*, 1829–1834. [CrossRef]
121. Blum, W.; Zhu, Q.; Markel, R.; McQueen, H.J. Geometric dynamic recrystallization in hot torsion of Al–5Mg–0.6Mn (AA5083). *Mater. Sci. Eng. A* **1996**, *A205*, 23–30. [CrossRef]
122. Hirsch, J.; Lucke, K. Mechanism of deformation and development of rolling textures in polycrystalline f.c.c. metals—I. Description of rolling texture development in homogeneous CuZn alloys. *Acta Metall. Mater.* **1988**, *36*, 2863–2882. [CrossRef]
123. Hirsch, J.; Lucke, K.; Hatherly, M. Mechanism of deformation and development of rolling textures in polycrystalline f.c.c. metals—III. The influence of slip inhomogeneities and twinning. *Acta Metall. Mater.* **1988**, *36*, 2905–2927. [CrossRef]
124. Konkova, T.; Mironov, S.; Korznikov, A.; Semiatin, S.L. Structural response of pure copper to cryogenic rolling. *Acta Mater.* **2010**, *58*, 5262–5273. [CrossRef]
125. Haase, C.; Barrales-Mora, L.A.; Roters, F.; Molodov, D.A.; Gottstein, G. Applying the texture analysis for optimizing thermomechanical treatment of high manganese twinning-induced plasticity steel. *Acta Mater.* **2014**, *80*, 327–340. [CrossRef]
126. Konkova, T.; Mironov, S.; Korznikov, A.V.; Korznikova, G.; Myshlyaev, M.M.; Semiatin, S.L. Grain structure evolution during cryogenic rolling of alpha brass. *J. All. Comp.* **2015**, *629*, 140–147. [CrossRef]

127. Odnobokova, M.; Belyakov, A.; Kaibyshev, R. Grain refinement and strengthening of austenitic stainless steels during large strain cold rolling. *Philos. Mag.* **2019**, *99*, 531–556. [CrossRef]
128. Yanushkevich, Z.; Belyakov, A.; Haase, C.; Molodov, D.A.; Kaibyshev, R. Structural/textural changes and strengthening of an advanced high-Mn steel subjected to cold rolling. *Mater. Sci. Eng. A* **2016**, *A651*, 763–773. [CrossRef]
129. Ray, R.K.; Jonas, J.J.; Hook, R.E. Cold rolling and annealing textures in low carbon and extra low carbon steels. *Int. Mater. Rev.* **1994**, *39*, 129–172. [CrossRef]
130. Wenk, H.-R.; Houtte, P.V. Texture and anisotropy. *Rep. Prog. Phys.* **2004**, *67*, 1367–1428. [CrossRef]
131. Kestens, L.A.I.; Pirgazi, H. Texture formation in metal alloys with cubic crystal structures. *Mater. Sci. Technol.* **2016**, *32*, 1303–1315. [CrossRef]
132. Zherebtsov, S.V.; Dyakonov, G.S.; Salem, A.A.; Malysheva, S.P.; Salishchev, G.A.; Semiatin, S.L. Evolution of grain and subgrain structure during cold rolling of commercial-purity titanium. *Mater. Sci Eng. A* **2011**, *A528*, 3474–3479. [CrossRef]
133. Dyakonov, G.S.; Mironov, S.; Zherebtsov, S.V.; Malysheva, S.P.; Salishchev, G.A.; Salem, A.A.; Semiatin, S.L. Grain-structure development in heavily cold-rolled alpha-titanium. *Mater. Sci. Eng. A* **2014**, *A607*, 145–154. [CrossRef]
134. Zherebtsov, S.V.; Dyakonov, G.S.; Salishchev, G.A.; Salem, A.A.; Semiatin, S.L. The influence of grain size on twinning and microstructure refinement during cold rolling of commercial-purity titanium. *Metall. Mat. Trans. A* **2016**, *47A*, 5101–5113. [CrossRef]
135. Li, S.; Beyerlein, I.J.; Bourke, M.A.M. Texture formation during equal channel angular extrusion of fcc and bcc materials: Comparison with simple shear. *Mater. Sci. Eng. A* **2005**, *A394*, 66–77. [CrossRef]
136. Beyerlein, I.J.; Tóth, L.S. Texture evolution in equal-channel angular extrusion. *Prog. Mater. Sci.* **2009**, *54*, 427–510. [CrossRef]
137. Kulitskiy, V.; Malopheyev, S.; Mironov, S.; Kaibyshev, R. Grain refinement in an Al-Mg-Sc alloy: Equal channel angular pressing versus friction-stir processing. *Mater. Sci. Eng. A* **2016**, *A674*, 480–490. [CrossRef]
138. Li, S.; Gazder, A.A.; Beyerlein, I.J.; Pereloma, E.V.; Davies, C.H.J. Effect of processing route on microstructure and texture development in equal channel angular extrusion of interstitial-free steel. *Acta Mater.* **2006**, *54*, 1087–1100. [CrossRef]
139. Yanushkevich, Z.; Mogucheva, A.; Tikhonova, M.; Belyakov, A.; Kaibyshev, R. Structural strengthening of an austenitic stainless steel subjected to warm-to-hot working. *Mater. Charact.* **2011**, *62*, 432–437. [CrossRef]
140. Dyakonov, G.S.; Mironov, S.; Semenova, I.P.; Valiev, R.Z.; Semiatin, S.L. Microstructure evolution and strengthening mechanisms in commercial purity titanium subjected to equal channel angular pressing. *Mater. Sci. Eng. A* **2017**, *A701*, 289–301. [CrossRef]
141. Zherebtsov, S.; Yurchenko, N.; Shaysultanov, D.; Tikhonovsky, M.; Salishchev, G.; Stepanov, N. Microstructure and mechanical properties evolution in HfNbTaTiZr refractory high-entropy alloy during cold rolling. *Adv. Eng. Mater.* **2020**, *22*, 2000105. [CrossRef]
142. Belyakov, A.; Tikhonova, M.; Dolzhenko, P.; Sakai, T.; Kaibyshev, R. On kinetics of grain refinement and strengthening by dynamic recrystallization. *Adv. Eng. Mater.* **2019**, *21*, 1800104. [CrossRef]
143. Dolzhenko, P.; Tikhonova, M.; Sakai, T.; Belyakov, A.; Kaibyshev, R. Dynamic recrystallization in austenitic stainless steel during hot working with decreasing deformation temperature. *Mater. Perform. Charact.* **2019**, *8*, 808–820. [CrossRef]
144. Torganchuk, V.; Vysotskiy, I.; Malopheyev, S.; Mironov, S.; Kaibyshev, R. Microstructure evolution and strengthening mechanisms in friction-stir welded TWIP steel. *Mater. Sci. Eng. A* **2019**, *A746*, 248–258. [CrossRef]
145. Hall, E.O. The deformation and ageing of mild steel: III Discussion of results. *Proc. Phys. Soc. B* **1951**, *64*, 747. [CrossRef]
146. Petch, N.J. The cleavage strength of polycrystals. *J. Iron Steel Inst.* **1953**, *174*, 25–28.
147. Schneibel, J.H.; Heilmaier, M. Hall-Petch breakdown at elevated temperatures. *Mater. Trans.* **2014**, *55*, 44–51. [CrossRef]
148. Belyakov, A.; Odnobokova, M.; Shakhova, I.; Kaibyshev, R. Regularities of microstructure evolution and strengthening mechanisms of austenitic stainless steels subjected to large strain cold working. *Mater. Sci. Forum* **2017**, *879*, 224–229. [CrossRef]
149. Takaki, S.; Akama, D.; Nakada, N.; Tsuchiyama, T. Effect of grain boundary segregation of interstitial elements on Hall–Petch coefficient in steels. *Mater. Trans.* **2014**, *55*, 28–34. [CrossRef]
150. Thompson, A.W. Substructure strengthening mechanisms. *Metall. Trans. A* **1977**, *8A*, 833–842. [CrossRef]
151. Estrin, Y.; Toth, L.S.; Molinari, A.; Brechet, Y. A dislocation density model for all hardening stages in large strain deformation. *Acta Mater.* **1998**, *46*, 5509–5522. [CrossRef]
152. Miller, A.K.; Sherby, O.D. On subgrain strengthening at high and low temperatures. *Scr. Metall.* **1976**, *10*, 311–317. [CrossRef]
153. Abson, D.J.; Jonas, J.J. The Hall-Petch relation and high-temperature subgrains. *Met. Sci. J.* **1979**, *4*, 24–28. [CrossRef]
154. Hughes, D.A.; Hansen, N. Microstructure and strength of nickel at large strains. *Acta Mater.* **2000**, *48*, 2985–3004. [CrossRef]
155. Hansen, N. Hall–Petch relation and boundary strengthening. *Scr. Mater.* **2004**, *51*, 801–806. [CrossRef]
156. Harrell, T.J.; Topping, T.D.; Wen, H.; Hu, T.; Schoenung, J.M.; Lavernia, E.J. Microstructure and strengthening mechanisms in an ultrafine grained Al-Mg-Sc alloy produced by powder metallurgy. *Metall. Mater. Trans. A* **2014**, *45A*, 6329–6343. [CrossRef]
157. Tanaka, Y.; Takaki, S.; Tsuchiyama, T.; Uemori, R. Effect of grain size on the yield stress of cold worked iron. *ISIJ Int.* **2018**, *58*, 1927–1933. [CrossRef]
158. Starink, M.J. Dislocation versus grain boundary strengthening in SPD processed metals: Non-causal relation between grain size and strength of deformed polycrystals. *Mater. Sci. Eng. A* **2017**, *A705*, 42–46. [CrossRef]
159. Dolzhenko, A.; Kaibyshev, R.; Belyakov, A. Tempforming as an advanced processing method for carbon steels. *Metals* **2020**, *10*, 1566. [CrossRef]

160. Mukherjee, J.K. Thermomechanical ausforming technique for producing substitute ultra high strength steels. In Proceedings of the Symposium on Metallurgy of Substitute Ferrous & Non-Ferrous Alloys, Jamshedpur, India, 27–30 April 1966; National Metallurgy Laboratory: Jamshedpur, India, 1966; pp. 156–161. Available online: http://eprints.nmlindia.org/3137 (accessed on 2 February 2022).
161. Schaller, F.W.; Schmatz, D.J. The inheritance of defects by martensite. *Acta Metall.* **1963**, *11*, 1193–1194. [CrossRef]
162. Kimura, Y.; Inoue, T.; Yin, F.; Tsuzaki, K. Inverse temperature dependence of toughness in an ultrafine grain-structure steel. *Science* **2008**, *320*, 1057–1060. [CrossRef]
163. Kimura, Y.; Inoue, T. Mechanical property of ultrafine elongated grain structure steel processed by warm tempforming and its application to ultra-high-strength bolt. *ISIJ Int.* **2020**, *60*, 1108–1126. [CrossRef]
164. Dolzhenko, A.; Yanushkevich, Z.; Nikulin, S.A.; Belyakov, A.; Kaibyshev, R. Impact toughness of an S700MC-type steel: Tempforming vs ausforming. *Mater. Sci. Eng. A* **2018**, *A723*, 259–268. [CrossRef]
165. Dolzhenko, A.; Yanushkevich, Z.; Kopteva, K.; Belyakov, A.; Kaibyshev, R. Effect of tempforming temperature on the microstructure and mechanical properties of a high-strength low-carbon steel. In Proceedings of the International Conference on Metallurgy and Materials, Conference Proceedings, Brno, Czech Republic, 22–24 May 2019; pp. 632–637. [CrossRef]
166. Dolzhenko, A.S.; Dolzhenko, P.D.; Belyakov, A.N.; Kaibyshev, R.O. Microstructure and impact toughness of high-strength low-alloy steel after tempforming. *Phys. Met. Metallogr.* **2021**, *122*, 1014–1022. [CrossRef]
167. Kaibyshev, O.A. *Superplasticity of Alloys, Intermetallics and Ceramics*; Springer: Berlin, Germany, 1992; p. 317. [CrossRef]
168. Zherebtsov, S.V.; Kudryavtsev, E.A.; Salishchev, G.A.; Straumal, B.B.; Semiatin, S.L. Microstructure evolution and mechanical behavior of ultrafine Ti-6Al-4V during low-temperature superplastic deformation. *Acta Mater.* **2016**, *121*, 152–163. [CrossRef]
169. Higashi, K. Positive exponent superplasticity in advanced aluminum alloys with nano or near-nano scale grained structures. *Mater. Sci. Eng. A* **1993**, *A166*, 109–118. [CrossRef]